NeuroImage 201 (2019) 116018

Contents lists available at ScienceDirect

NeuroImage

journal homepage: www.elsevier.com/locate/neuroimage

# Quantifying deep grey matter atrophy using automated segmentation approaches: A systematic review of structural MRI studies

Alex M. Pagnozzi *, Jurgen Fripp, Stephen E. Rose

*CSIRO Health and Biosecurity, The Australian e-Health Research Centre, Brisbane, Australia*

ARTICLE INFO

*Keywords:*
Magnetic resonance imaging
Deep grey matter
Subcortical anatomies
Segmentation

ABSTRACT

The deep grey matter (DGM) nuclei of the brain play a crucial role in learning, behaviour, cognition, movement and memory. Although automated segmentation strategies can provide insight into the impact of multiple neurological conditions affecting these structures, such as Multiple Sclerosis (MS), Huntington's disease (HD), Alzheimer's disease (AD), Parkinson's disease (PD) and Cerebral Palsy (CP), there are a number of technical challenges limiting an accurate automated segmentation of the DGM. Namely, the insufficient contrast of T1 sequences to completely identify the boundaries of these structures, as well as the presence of iso-intense white matter lesions or extensive tissue loss caused by brain injury. Therefore in this systematic review, 269 eligible studies were analysed and compared to determine the optimal approaches for addressing these technical challenges. The automated approaches used among the reviewed studies fall into three broad categories, atlas-based approaches focusing on the accurate alignment of atlas priors, algorithmic approaches which utilise intensity information to a greater extent, and learning-based approaches that require an annotated training set. Studies that utilise freely available software packages such as FIRST, FreeSurfer and LesionTOADS were also eligible, and their performance compared. Overall, deep learning approaches achieved the best overall performance, however these strategies are currently hampered by the lack of large-scale annotated data. Improving model generalisability to new datasets could be achieved in future studies with data augmentation and transfer learning. Multi-atlas approaches provided the second-best performance overall, and may be utilised to construct a "silver standard" annotated training set for deep learning. To address the technical challenges, providing robustness to injury can be improved by using multiple channels, highly elastic diffeomorphic transformations such as LDDMM, and by following atlas-based approaches with an intensity driven refinement of the segmentation, which has been done with the Expectation Maximisation (EM) and level sets methods. Accounting for potential lesions should be achieved with a separate lesion segmentation approach, as in LesionTOADS. Finally, to address the issue of limited contrast, R2*, T2* and QSM sequences could be used to better highlight the DGM due to its higher iron content. Future studies could look to additionally acquire these sequences by retaining the phase information from standard structural scans, or alternatively acquiring these sequences for only a training set, allowing models to learn the "improved" segmentation from T1-sequences alone.

## 1. Introduction

The deep grey matter (DGM) nuclei of the brain are central to a number of neural circuits that connect a range of locations on the cerebral cortex. Collectively, these structures play a crucial role in the learning, planning and execution of behavioural responses (Cools et al., 2002; Haber and Calzavara, 2009), cognition (Babikian et al., 1990), movement initiation (Boecker et al., 2008), sensorimotor coordination (Grahn et al., 2008), spatial localisation (Cook and Kesner, 1988) and memory (Graybiel, 2000). The anatomies which constitute the DGM include the caudate nucleus, the lenticular nucleus (which comprise of the putamen and globus pallidus), and the thalamus, which are illustrated in Fig. 1. The putamen and globus pallidus are two lenticular, iron-rich structures (Aquino et al., 2009), which consist of both inhibitory and excitatory pathways connecting to the cerebral cortex and thalamus, and subserve general motor behaviour, including motivation, planning and coordination (Smith et al., 1998). With the inclusion of the caudate nuclei, which are long, thin, C-shaped structures, these

* Corresponding author. Australian e-Health Research Centre, Level 5, UQ Health Sciences Building, Royal Brisbane and Women's Hospital, Herston, QLD, 4029, Australia.
*E-mail address:* Alex.Pagnozzi@csiro.au (A.M. Pagnozzi).

https://doi.org/10.1016/j.neuroimage.2019.116018
Received 18 February 2019; Received in revised form 1 July 2019; Accepted 12 July 2019
Available online 15 July 2019

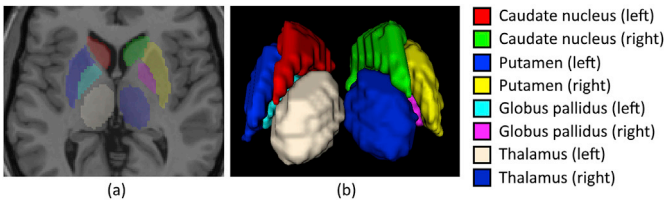


**Fig. 1.** (a) The Colin 27 atlas with overlayed DGM labels obtained from the Automated Anatomical Labelling (AAL) atlas, and (b) a 3D visualisation of these DGM structures obtained using ITK-SNAP (Yushkevich et al., 2006).

anatomies largely form the basal ganglia, which has an important role in memory and learning (Graybiel, 1995). The thalamus consists of multiple internal nuclei, which are involved in modulating and relaying information, including visual, auditory, somatosensory information, as well as cortico-cortical communication (Sherman and Guillery, 2002). The interruption of this basal ganglia-thalamocortical loop can lead to either hyper- or hypokinesia, highlighting the importance of these structures.

There are numerous brain pathologies which impact the DGM, most commonly Multiple Sclerosis (MS) which affect the subcortical structures through formation of focal demyelinating lesions and diffuse neurodegeneration (Haider et al., 2014). The importance of subcortical structures in the pathology of MS has been strengthened by the observed associations between the DGM and memory impairment (Benedict et al., 2009) and clinical disabilities (Haider et al., 2014). Neurodegeneration associated with Huntington's disease (HD) has revealed atrophy in the cortical and DGM (Ruocco et al., 2008), with such severity that it can affect the anatomical alignment necessary for methods like Voxel Based Morphometry (VBM). Abnormal iron accumulation in the DGM has been associated with Alzheimer's disease (AD) and Parkinson's disease (PD) (Pal et al., 2011), which in turn lead to formation of protein deposits and subsequent neurodegeneration. Indeed, reduced amygdala, caudate, pallidum and putamen volumes were observed in AD (de Jong et al., 2008). Patterns of hypoxic-ischemic injury predominantly involve the subcortical white and grey matter, with heterogeneous injury in the basal ganglia observed in some developmental conditions such as dyskinetic Cerebral Palsy (CP) (R.Aravamuthan and L.Waugh, 2016). Furthermore, preterm infants born at 24–33 weeks gestation showed reduced thalamic and lentiform volumes, with more marked differences observed with greater prematurity, impacting global cerebral development (Boardman et al., 2006). These findings highlight the importance of obtaining segmentations of the subcortical structures in order to quantify potential atrophy caused by these pathologies. Segmentation of the DGM is also critical in other applications, such as radiotherapy therapy planning for patients with brain tumours, so that tumours can be sufficiently irradiated whilst sparing the DGM (Dolz et al., 2015).

As such quantifying DGM volume and shape may be important in the diagnosis of these conditions, or in estimating patient prognosis. However performing these quantifications manually requires laborious annotation of medical images, which is infeasible. Automated methods are therefore necessary to quantify these important structures, however there are a number of technical challenges limiting an accurate automated segmentation of the DGM. For instance, the boundary of the thalamus is not often visible from structural magnetic resonance imaging (MRI) alone due to the heterogeneous appearance of its internal subnuclei and myelinated laminae (Morel et al., 1997), necessitating the use of labelled atlases to provide information on standard DGM shape. This is true for even images from healthy individuals, however the inclusion of potential injury can further obfuscate these structures. Injury to the white matter (WM), such as periventricular leukomalacia (PVL), leads to neurodegeneration in the WM, leading to a reduction in intensity on T1-weighted MRIs which may become isointense with the DGM. More severe forms of PVL lead to cystic cerebrospinal fluid (CSF)-filled regions, which can replace whole sections of the DGM. Many of these constraints in DGM segmentation exist in cohorts with heterogeneous brain injury, such as CP. Illustrations of these potential difficulties from a CP cohort is illustrated in Fig. 2.

Many methods have been proposed for the task of DGM segmentation, which can broadly be divided into three categories: atlas-based approaches, algorithmic-based approaches and learning-based approaches. Atlas-based approaches are the most frequently used method, which use one or more labelled images as a basis for segmenting the DGM. To accommodate anatomical variation, different registration paradigms exist to allow more extreme deformations of the atlas to fit the target (Djamanakova et al., 2013), as an accurate alignment of the atlas is critical for the performance of these methods. In addition, multiple atlases can be used, with specific atlases being selected based on a similarity metric, or labels from multiple aligned atlases being fused together to produce a final segmentation. Algorithmic-based approaches cover several different methods, including the Expectation Maximisation (EM) method (Dempster et al., 1977), which uses the Bayesian framework to perform tissue classification using Gaussian distributions of MRI intensities. Another set of algorithms called Statistical Shape Models (SSMs) model shape variations from a training set of aligned segmentations (Heimann and Meinzer, 2009), and can additionally include appearance information from sMRI. Combined with the Bayesian framework, shape models provide a basis for the freely available FIRST software for DGM segmentation (Patenaude et al., 2011). Deformable models are another set of algorithms, which include active contours (Kass et al., 1988) and level sets (Osher and Sethian, 1988), and both deform a curve or surface based on external image and internal shape parameters. Algorithmic approaches are flexible and can adjust to variable anatomy, however also require an accurate initialisation using accurate *a priori* information. Finally, learning-based approaches include Support Vector Machines (SVM) (Cortes and Vapnik, 1995), Artificial Neural Networks (ANN) and Convolutional Neural Networks (CNN) which are a variant of ANNs that train 3D convolutions applied to MRI data. Using a training set of data with ground truth segmentations, these methods learn associations between image features and output labels encoded in the weights within nodes of the network. The performance of these methods has been bolstered in recent years with advances in computing power, however the generalisability of these approaches depends on the size and the variability contained within the training set necessary to construct these models.

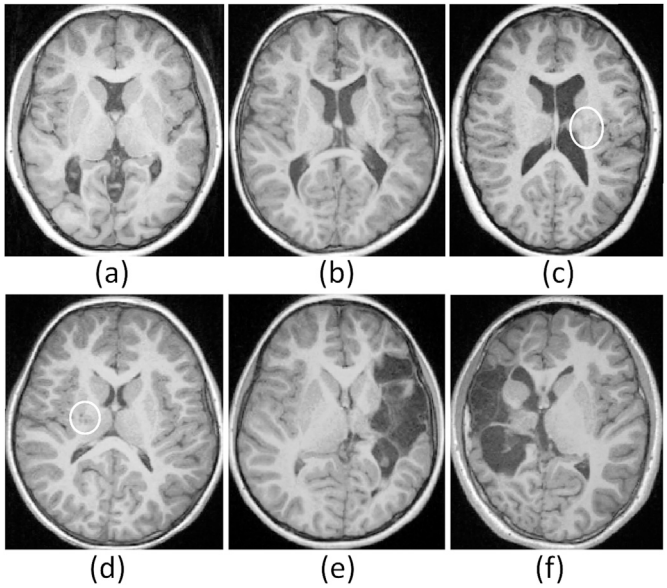


**Fig. 2.** Axial MPRAGE slices of 6 children with Cerebral Palsy (CP) illustrating the DGM structures; (a–b) show healthy variation in brain anatomy, (c–d) contain white matter lesions (highlighted by the white circles) which are isointense with the grey matter, and (e–f) which contains severe tissue loss leading to partial loss of the DGM structures.

Therefore, this systematic review aims to summarise the studies that perform an automated segmentation of the DGM, in order to identify the current state-of-the-art approaches for subcortical segmentation. Among the reviewed studies, particular focus is paid to methods that can overcome the numerous technical limitations caused by pathological variations, to elucidate approaches that can be routinely applied to various clinical cohorts. To review the large number of techniques that have been proposed for this task, this review focusses on automated approaches that require no manual intervention, and that only utilise sMRI, as unlike diffusion and functional MRI studies, sMRI has standardised sequences routinely used in the clinical setting. The advantages and limitations of the different methods for DGM segmentation are then summarised, including the different software packages designed for DGM segmentation, and the findings for each approach are homogenised and compared. Finally, future directions for the task of DGM segmentation are proposed for addressing the potential technical difficulties of automated DGM segmentation.

## 2. Selection criteria

A systematic search was conducted for relevant studies in four databases; PubMed, Web of Science, IEEE Xplore and Scopus, on 25 April 2019. The key search terms were: ((‘deep gray matter’ OR ‘deep grey matter’ OR ‘subcortical nuclei’ OR ‘subcortical structures’) AND ‘segmentation’ AND (‘magnetic resonance imaging’ OR ‘MRI’)). A full-text search was performed on all databases. Additionally, manual searches were conducted among the reference sections of the retrieved studies and reviews. The inclusion and exclusion criteria for the current review applied to the retrieved articles are listed below.

Inclusion criteria:

i. Studies include human participants
ii. Articles describing methods for automated DGM segmentation
iii. Methods involve segmentation of one or more deep grey matter structures (illustrated in Fig. 1)
iv. Data utilises structural MRI sequences

Exclusion criteria:

i. Articles published in languages other than English
ii. Articles describing manual or semi-automated segmentation approaches
iii. Methods do not segment one or more of the deep grey matter structures illustrated in Fig. 1 (such as the hippocampus and subthalamic nucleus)
iv. Methods that do not perform volumetric segmentation of deep grey matter structures (such as VBM which measures voxel-wise grey matter density)
v. Study was a review or meta-analysis

Of the 303 potentially relevant studies identified from PubMed, 484 from Web of Science, 44 from Scopus, 23 from IEEE Xplore and a further four articles added manually from screened review articles, a total of 269 studies were selected for review. An in-depth detail of the excluded studies, and the reasons for exclusion, are shown in Fig. 3. A complete outline of these 269 articles, including descriptions of the study motivation, data, methods and findings, are provided in Supplementary Tables 1 and 2.

## 3. Review

The review of these 269 articles is provided below, with the reviewed methods classified into three groups. In the first section atlas-based approaches are discussed, consisting of methods that largely rely on propagated atlas labels, and includes single- and multi-atlas techniques, registration approaches for optimal atlas alignment, as well as different atlas selection and label fusion approaches for multi-atlas methods, and construction of tailored atlases for specific cohorts. Methods that instead utilise models largely driven by image intensity information, such as EM, or *a priori* shape information, such as shape models, or both, such as appearance models, level sets and active contours, are discussed in the algorithmic-methods section. Finally, methods that instead learn accurate anatomical segmentations from a library of existing segmentations, including ANNs and CNNs, are discussed in the learning-based approaches section. The reviewed studies that utilise specific implementations of the above methods are detailed in Supplementary Table 1. In the following section, a discussion of the different freely available software packages for DGM segmentation is provided, with the summary of reviewed studies that used these software packages provided in Supplementary Table 2. An overview of the various applications of DGM segmentation is then provided, followed by a discussion of the reviewed methods, where methodological recommendations are made in light of the technical challenges in this area.

### 3.1. Atlas-based approaches

The most common type of methods used for DGM segmentation utilise atlases containing labels for the DGM, which are then aligned via a registration paradigm in order to identify these anatomies in a target image (de Jong et al., 2017), as shown in Fig. 4. Atlases can be constructed from one or more medical images along with corresponding labelled images, which provide *a priori* information of tissue location. This information is crucial to the task of DGM segmentation as it allows distinction of the DGM structures from the cortical grey matter (GM) which have similar intensities in sMRI, and would otherwise be identical to intensity-driven algorithms such as Expectation Maximisation (EM). Atlases constructed from multiple images typically involve each image being elastically deformed to each other, allowing an image of the “average” anatomy to be identified as an average transformation of a given reference image (Joshi et al., 2004). In several studies, creation of a cohort specific atlas was performed to improve the accuracy of subcortical segmentations (Lalys et al., 2010). For instance, a 7-year old atlas was constructed using manually labelled DGM templates for the Pediatric Subcortical Segmentation Tool (PSST), which was shown to outperform both FIRST and FreeSurfer for the segmentation of DGM in infants (Loh et al., 2016). Furthermore, using a group-wise registration approach to create an unbiased template from T1 and T2-weighted 7T MRI data, segmentation accuracy of the globus pallidus using this unbiased template was shown to outperform both single and multi-atlas approaches (Wang et al., 2016).

The accuracy of atlas-based approaches critically rely on how accurately the atlas is aligned with the target image, hence many studies have attempted to optimise the registration paradigm in order to improve the DGM segmentation. Atlas registration using the Insight Segmentation and Registration Toolkit (ITK) (Wu et al., 2006) was used to align segmentations of the DGM provided by the AAL atlas (Tzourio-Mazoyer et al., 2002) to characterise subcortical structure in both adults (Dombrovski et al., 2012) and infants (Scott et al., 2013). A fast, elastic matching algorithm was developed in one study (Warfield et al., 1995), with similar registration algorithms used in other studies (Grachev et al., 1999; Iosifescu et al., 1997), all which utilise nonlinear transformations to account for potential anatomical variability in the DGM. Another non-rigid registration approach called the Thirion’s demons algorithm (Thirion, 1998) utilises optical flow based on local image characteristics to achieve a fast alignment between image and atlas, however does not guarantee conservation of topology. Therefore Demon’s registration was followed in one study by topological correction based on *a priori* shape information to achieve an accurate DGM segmentation (Lin et al., 2010), whilst in another study Demon’s was optimised using shape and intensity information from the propagated DGM labels (XiangBo Lin et al., 2008). Atlas registration was used in one study to generate a DGM probability map, to then use a sparse representative classifier to refine the subcortical

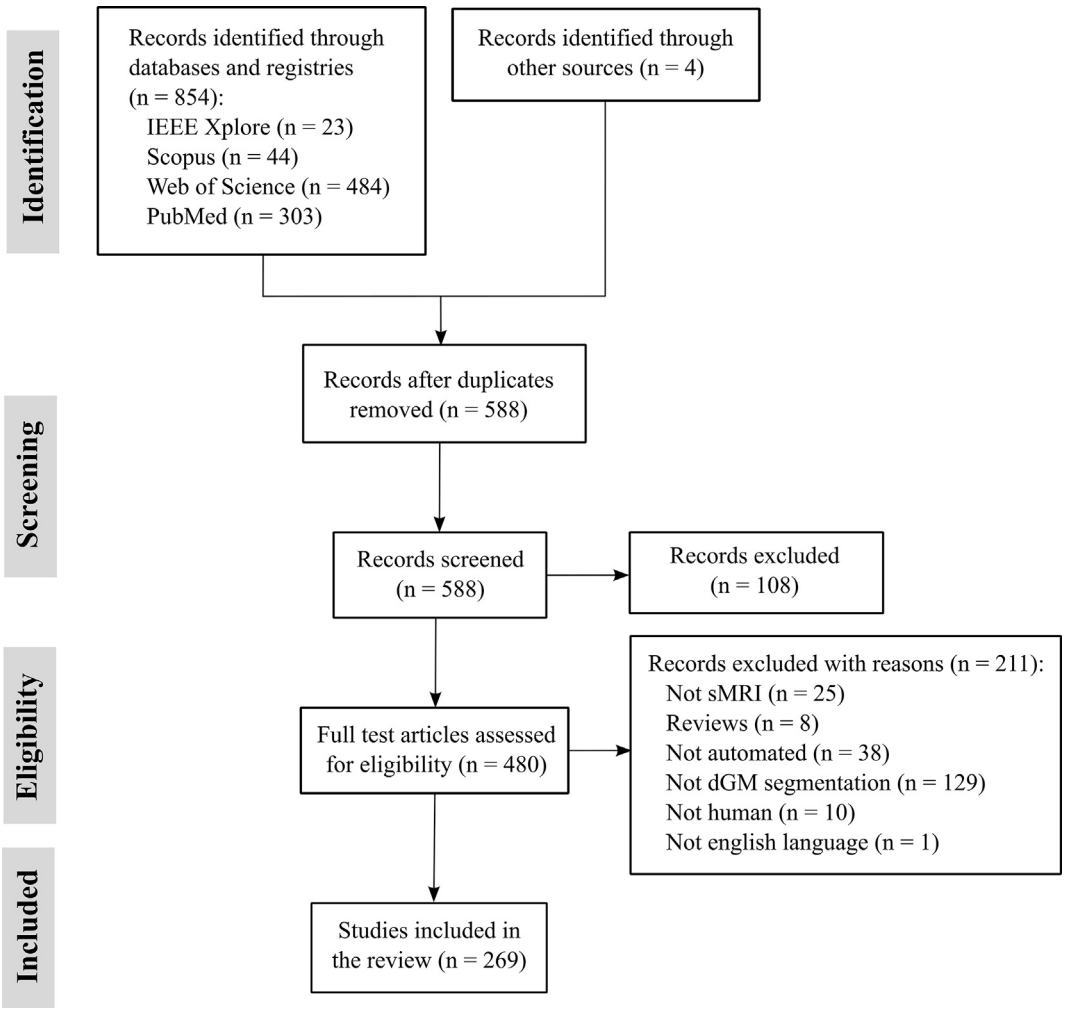


**Fig. 3.** Study flow and reasons for exclusion.

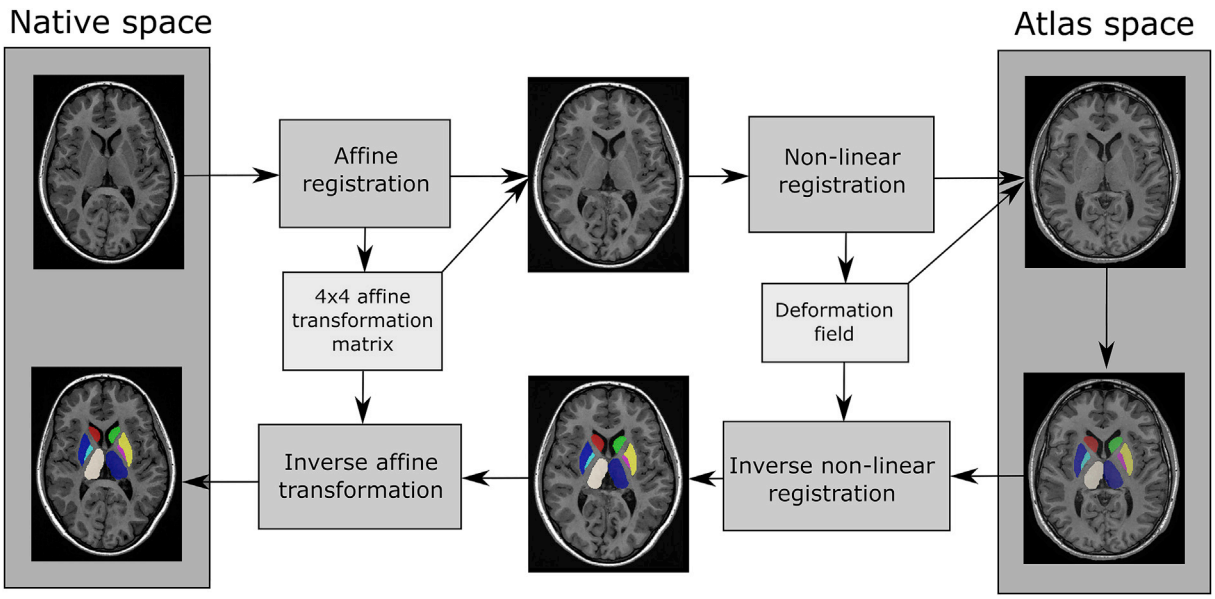


**Fig. 4.** Flowchart illustrating single-atlas approach for labelling a target image.

structures, which outperformed both FIRST and FreeSurfer and achieved comparable performance to the latest DL architectures (Liu et al., 2019). Whilst registration approaches can overcome variations in anatomy across the population, it may be challenging to find an accurate alignment in patients with severe brain injury and tissue loss. Large-deformation diffeomorphic metric mapping (LDDMM) is a non-rigid registration algorithm capable of aligning significantly different anatomy (Beg et al., 2005), and was used to transform a subcortical atlas generated by FreeSurfer to segment the DGM in several studies (Garg et al., 2015; Khan et al., 2009, 2008; Khan and Beg, 2009). As such, LDDMM may be one potential approach to accurately propagate labels from a healthy atlas to a patient with severe brain injury. When comparing registration approaches, studies identified non-linear approaches on a 1 mm grid (Chakravarty et al., 2008) outperformed both linear and piece-wise linear techniques (Chakravarty et al., 2009), while in another study the iteratively non-rigid propagation of atlas labels between target images, as opposed to atlas to target propagation, was proposed for DGM segmentation (Sullivan et al., 2011). In a comparison of several non-linear registration approaches, FSL FNIRT, SPM Segment and ANTs Symmetric Normalization showed the greatest segmentation accuracy of the internal pallidum (Ewert et al., 2019).

Improving atlas alignment can be achieved with algorithms that perform several registration steps or incorporate multiple sources of information, such as additional MR sequences or surface landmarks. An affine alignment followed by a deformable transformation yielded the best performance for DGM segmentation (Yousefi et al., 2012), whilst in another study the sequential use of rigid, affine and Thirion's demons non-linear deformations, each providing a more precise alignment of the atlas labels, was utilised in two studies to segment the DGM (Linguraru et al., 2007, 2006). Ensuring consistency between the forward and reverse transformations between atlas and target can be achieved with a symmetric consistent diffeomorphic registration, which was shown to outperform B-spline based free form deformation and ITK Demon's registration for the segmentation of the DGM (Tao et al., 2009). Subcortical alignment has been further improved in several studies using several approaches, including combining volumetric and surface registration (Postelnicu et al., 2009), performing two-way free-form deformations to extract a regional measure of registration accuracy (Heckemann et al., 2009) and initialising an inverse-consistent registration with landmarks and utilising intensity information from T1, T2 and PD sequences (Magnotta et al., 2003). Unlike landmark-driven correspondences, which provide anatomical relevance but may be irregularly distributed, and intensity-driven correspondences, which provide distributed warps but may not be anatomically feasible, one approach iterates between segmentation of the target from the atlas, anatomical correspondence from these segmentations, and atlas-to-target deformation to determine an optimal correspondence that is robust to brain injury (Meier and Fisher, 2005).

Several approaches use multiple atlases, each of which can be registered to a target as illustrated in Fig. 5, to yield improved segmentation results. Although this requires construction of multiple atlases and is more computationally intensive due to several registrations being necessary, it can potentially model a greater amount of anatomical variability by utilising atlases with differing structure. Indeed, an improved segmentation of the DGM was obtained with more atlases used in a multi-atlas approach when applied to the OASIS dataset ($n = 20$) (Gorthi, 2016). Several multi-atlas methods exist, including the freely-available CRUISE approach which uses 45 images from the OASIS dataset (Huo et al., 2016), as well as the non-rigid registration of thirty atlases applied to an infant cohort (Gousias et al., 2008). In the MAGeT multi-atlas approach (Chakravarty et al., 2006), multiple manual segmentations are nonlinearly registered to the target, which have been used for DGM segmentation in multiple studies (Magon et al., 2015; Raznahan et al., 2014; D Sussman et al., 2016; Dafna Sussman et al., 2016; Sussman et al., 2017, 2015). Using a big data registration enhance (BRDE) multi-atlas approach, multiple atlases (consisting of over 5000 3T and 7T images) are registered to a target using ANTs Symmetric Normalization algorithm to obtain accurate subfield segmentations of the thalamus (Bao et al., 2019). Among the reviewed studies, the average Dice Similarity Coefficient (DSC) across all DGM structures for the multi-atlas approaches was 0.832, which was slightly above the reported average DSC for all single-atlas approaches (0.808).

Multi-atlas approaches may preferentially select specific atlases for label propagation, which can reduce computational complexity. The simplest approach is to perform a random selection of the atlases (Lötjönen et al., 2010), however selecting atlases based on their similarity to the target image may provide a more accurate labelling. For instance, an optimal atlas-selection strategy based on local registration accuracy as measured by normalized mutual information, was shown to outperform a single atlas for DGM segmentation (Wu et al., 2007). The AutoSeg toolkit uses a directed graph was constructed to identify the registered atlases that were most similar template based on intensity and

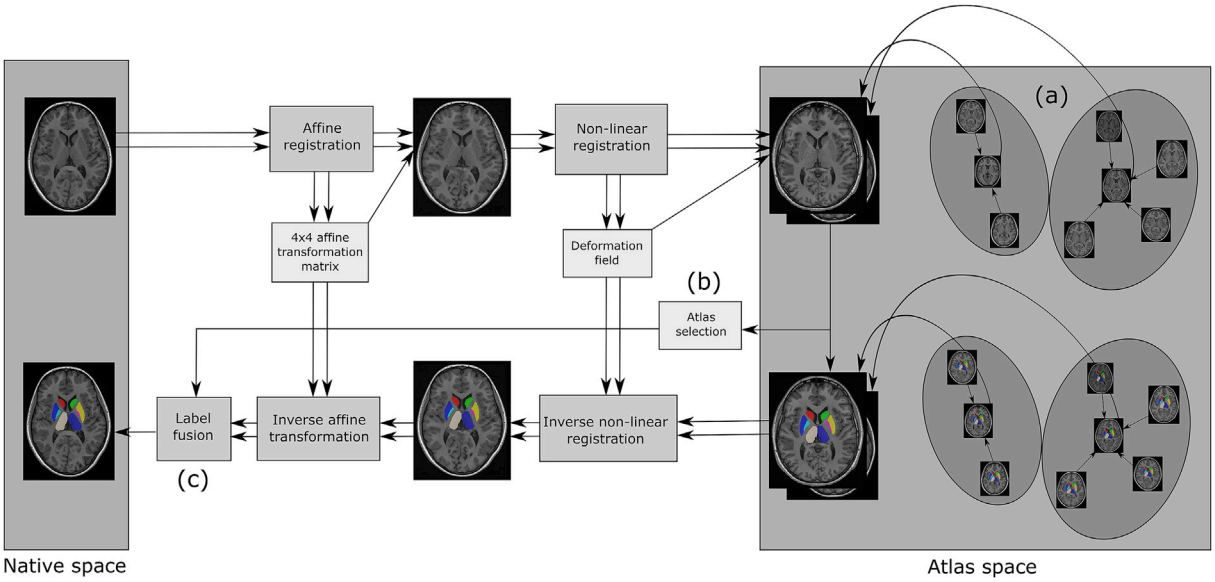


**Fig. 5.** Flowchart of multi-atlas methods, including (a) atlas clustering to minimise the number of target-to-atlas registrations necessary, (b) atlas selection which may either be binary or continuously weighted based on the similarity to the target, and (c) label fusion of multiple transformed atlas labels.

shape, with the most similar atlases contributing to a majority voting scheme, which has been evaluated on subcortical structure segmentation (Wang et al., 2014). Co-registered atlases may also be clustered, providing an efficient strategy to find the most similar exemplar atlas for improved segmentation accuracy (Wu et al., 2016). Atlas clustering was performed based on the affine transform in another approach to reduce computational complexity, which was then followed by non-rigid registration of the clusters to obtain a segmentation of the DGM (Keuken et al., 2014).

As opposed to atlas selection, different approaches have been proposed for combining multiple sets of labels from several aligned atlases to achieve a final segmentation. By performing separate registrations for each atlas prior to label fusion, greater anatomical variability can be captured, as well as improved robustness against potential registration failures. Whilst majority voting is the simplest label fusion method, which selects the most frequent label from the propagated atlases, it may slightly oversegment structures (Huo et al., 2015). Weighted voting instead incorporates intensity information by up-weighting atlases more similar to the target anatomy in the voting procedure, which can be performed jointly by considering pairwise atlas correlations when estimating label weights (Wang and Yushkevich, 2013b). This weighted fusion strategy is performed in MAGeT (Chakravarty et al., 2013), yielding a final segmentation that better accounts for anatomical variability than a single atlas with a single segmentation. Learning likelihoods for labelling (L3) is another label fusion approach utilising spatial and intensity information to achieve subcortical segmentation (Weisenfeld and Warfield, 2011). Optimal atlas and label selection of multiple diffeomorphically warped atlases has also been achieved with the EM algorithm to provide a posteriori estimate of the DGM segmentation (Lotjonen et al., 2009; X. Tang et al., 2013). Studies comparing label fusion methods found generative label fusion outperforming majority voting and STAPLE (Iglesias et al., 2015), while in another study Log-Odds was shown to outperform Tri-Linear and Nearest neighbour as well as FreeSurfer segmentations for the DGM (Sabuncu et al., 2010). Alternatively, additional post-processing steps can be implemented to further refine the fused labels to obtain a finalised segmentation. In several studies, the EM has been used either to perform label fusion (Keuken et al., 2014), or to refine the fused labels, which in the latter case was found to outperform FIRST and FreeSurfer on both paediatric and elderly datasets (Tang et al., 2015). In another approach, the level set function was used to optimise segmentations based on measures of DGM shape, which was then used to iteratively propagate a set of labels across an ensemble of data (Raviv et al., 2009; Riklin-Raviv et al., 2010). Other post-processing approaches used in DGM segmentation include MRF and graph cuts (Wolz et al., 2009), as well as conversion of the DGM segmentations to 3D triangulated meshes to perform mesh smoothing and generate smoother segmentations (Tang et al., 2018).

Although T1-weighted sequences reflect overall cyto- and myeloarchitecture (Eickhoff et al., 2005), many segmentation approaches utilise multiple MR sequences in order to better define the boundaries of the DGM that are not typically visible on T1-weighted MRI, specifically that of the thalamus. Fluid Attenuated Inversion Recovery (FLAIR) sequences can better visualise periventricular lesions, and were used alongside T1 in one study for the alignment of a DGM atlas using nonlinear symmetric registration (Spilling et al., 2017). FLAIR, T1- and T2-weighted sequences were used in another study which utilised automated segmentations of internal nuclei, ventricles and cortical boundary to better guide the non-rigid registration (Linguraru et al., 2006). Alternate measures such as R1 relaxation, which is a function of both iron and macromolecule concentration and T2*/Quantitative Susceptibility Mapping (QSM) provide information on magnetic field inhomogeneities caused by concentration of iron (Sato et al., 2017; Stüber et al., 2014). As the subcortical GM is iron-rich (Wang and Liu, 2015), these iron-based MR sequences can help provide extra contrast to delineate the boundaries of the DGM. Both T1-, T2*- and T1-T2*-fusion weighted sequences were shown to provide sufficient anatomical contrast, allowing the DGM and even subthalamic nuclei to be segmented using a multi-atlas segmentation strategy (Xiao et al., 2017). Using a multi-atlas segmentation strategy that facilitates supervoxel-wise correspondence to label pathological tissue appearances in patients with brain tumours (Wang and Yushkevich, 2013a), T1-weighted, R2* and QSM sequences were aligned and used for DGM segmentation (Fujiwara et al., 2017). By including R2*-weighted or QSM sequences in addition to a T1 for a multi-atlas approach showed either combination of sequences outperformed FSL's FIRST in DGM segmentation accuracy (Cobzas et al., 2015). In one study, the T1- and T2-weighted EVE atlas was extended with the QSM to achieve an accurate segmentation of the DGM (Lim et al., 2013), highlighting the potential utility of the QSM sequence.

Accounting for the temporal development of the brain is crucial in several contexts, particularly for imaging of infants where in the first months the convolution of the cortical surface of the brain increases significantly (Shi et al., 2011), necessitating the use of multiple atlases representing different time points. Imaging during early development is challenging due to the change in WM contrast from being hypointense relative to GM before 8 months of age due to lack of myelin at this stage of development, to being isointense to GM around 9 months, and finally being hyperintense relative to GM when fully myelinated after approximately 10 months (Prastawa et al., 2005). To overcome these challenges, spatio-temporal atlases have been constructed, which encode both variable anatomy as well as longitudinal development (Habas et al., 2010a, b). Registration of a spatio-temporal atlas was performed on a fetal MRI cohort to quantify longitudinal volume changes of the DGM (Scott et al., 2011). In neonatal MRIs too, spatio-temporal atlases plays an important role in providing the correct *a priori* information of brain structure, for DGM to then be segmented using the EM framework (Liu et al., 2016). Atlases modelling brain development across the lifespan have been proposed, which additionally utilise the QSM modality to include a DGM map including sub-thalamic parcellations (Zhang et al., 2018).

### 3.2. Algorithmic-based approaches

Atlases may not be available in all cases, due to limited annotated data, or difficulty in aligning different anatomy or potential brain injury using registration techniques. Algorithmic approaches in this review refer to methods that instead rely on image features such as the image intensity or texture of the DGM, although most of these techniques still require spatial *a priori* information. Early atlas-free classification algorithms such as k-nearest neighbour (k-NN) (Vinitski et al., 1999, 1997) used manually derived seed points as *a priori* information, and as well as gadolinium enhanced T1-MRI to better resolve the DGM in patients with brain tumours. Automated k-NN trained on manual segmentations was used with principal component discriminant analysis (PCDA) to achieve a segmentation of the DGM using the Bayes decision rule (Larobina et al., 2015). Algorithmic approaches have also been developed specifically for neonatal MRIs, where the DGM appears as a singular region of grey matter, with reduced T2-weighted intensities compared to cortical GM. Hence in one study, co-registered T1 and T2 sequences have been used to isolate the DGM collectively as darker T2 intensities following an intensity-driven segmentation of the WM/GM/CSF in infants (Kuklisova-Murgasova et al., 2011), while in another study these darker T2 intensities were extracted with the watershed algorithm, followed by morphological post-processing to obtain the DGM (Gui et al., 2012).

The EM algorithm uses Gaussian distributions to fit the different tissue classes (Dempster et al., 1977), and is often interleaved with Hidden Markov Random Fields (MRF) to obtain a spatially consistent segmentation. EM-MRF has shown robustness to intensity non-uniformity and noise with a low computational time (Benoit Scherrer et al., 2009), however there remains difficulty in segmenting DGM from intensity and textural features alone. Instead, leveraging spatial *a priori* information from atlases can help to delineate these structures even in cases when the boundary is not visible in the standard T1-weighted MR images. For instance, EM-MRF was used in combination with tissue priors from

multiple labelled atlases to provide a segmentation of the DGM (Makropoulos et al., 2014), the method for which was revised and improved on a larger cohort (Makropoulos et al., 2016). Similar approaches have used aligned atlases of the entire DGM (B. Scherrer et al., 2009; Shichun Peng and Rajapakse, 2002) or one specific anatomy, such as the thalamus (Pohl et al., 2006). DGM labels from the ICBM template were used along with T2-weighted and FLAIR sequences to correctly classify the DGM from both isointense cortical GM and MS lesions (Datta and Narayana, 2013). In more challenging cohorts, construction of specific atlases may be necessary to provide an accurate initialisation for EM. For instance, a probabilistic fetal DGM atlas was constructed using mutual-information based registration of multiple manual DGM segmentations, in order to initialise EM (Habas et al., 2010a,b). In another study the symmetric registration of a neonatal atlas was used prior to EM, after which post-processing correction was performed using level sets (Metzger et al., 2016). Generalised EM modelling has also been used to deform a 3D mesh, propagated from an aligned atlas, to fit the target DGM based on image intensities as well as internal shape properties to prevent tearing and folding (Puonti et al., 2013). In another classification algorithm called Random Forests (RF) (Brieman et al., 2001), textural features from both sMRI and DTI were identified on a training set with manual segmentations of sub-thalamic regions to achieve an automated parcellation of the thalamus (Stough et al., 2013).

Unlike EM which is driven by intensity distributions, another class of algorithms called Statistical Shape Models (SSM) instead use shape information and variability learned on a training set to deform a statistical model and produce an optimal segmentation on a test image (Heimann and Meinzer, 2009). To achieve this, the DGM structures are represented as a point distribution model (PDM), and the point-wise correspondence between multiple segmentations can the obtained using a piecewise linear transformation model. Variations in shape can be reflected as different 'modes' in the model, allowing the PDM to be then deformed down these modes to optimally align to a target image, producing a final segmentation. In a series of studies, PDMs constructed on a training set, as well as atlas information based on distance to subcortical structures, were used to initialise a mesh model of the DGM to a test image, and following model optimisation showed improved DGM segmentation accuracy (Akhondi-Asl and Soltanian-Zadeh, 2010; Akhondi Asl and Soltanian-Zadeh, 2008; Akhoundi-Asl and Soltanian-Zadeh, 2007). Several modifications of this standard SSM methodology exist, including using a LogOdds representation of shape to generate a PDM (Pohl et al., 2007), and extending the PDM methodology to characterising shape variability at different scales (Cerrolaza et al., 2015). PDM deformation can also be driven by Fractional Anisotropy (FA) from diffusion MRI in addition to T1-weighted MRI (Visser et al., 2016), while initial alignment of the subcortical shape prior can be further refined using RF feature learning, which was found to outperform FreeSurfer and FIRST (Guo et al., 2017). In several studies, adjacent non-DGM structures can be included in the PDM, such as the lateral ventricles, cerebellum and brainstem, whose addition can increase the robustness of model initialisation, which has been demonstrated on a cohort with traumatic brain injury (TBI) (Zagorchev et al., 2016). In another approach, the deformation of the PDM additionally incorporated boundary detection based on the image gradient to optimally fit the PDM in the target image whilst leveraging clearly separable, adjacent structures such as the lateral ventricles. This approach has been demonstrated on numerous datasets and was shown to outperform both FIRST and FreeSurfer (Wenzel et al., 2018).

Active Appearance Models (AAM) are an extension of SSMs, which additionally incorporate image intensity in the optimisation of the shape model and refinement of the PDM landmarks in the target image (Cerrolaza et al., 2012). AAMs have been found to perform similarly to intensity-based tissue classification with label fusion for the task of DGM segmentation (Babalola et al., 2008). As an accurate initialisation of both SSMs and AAMs are important for good performance, in one study an optimised model initialisation was used which included registration, template matching and additional heuristics, prior to AAM optimisation (Babalola and Cootes, 2010). The AAM framework is utilised by the FSL FIRST software (Patenaude et al., 2011), which aligns the pre-trained mesh surfaces of the DGM in a target image in a two-step process, global linear alignment followed by a regional affine alignment, allowing this approach to be used for a wide variety of clinical applications.

Unlike SSMs which utilise modes of variation observed on a training set to transform the target shape, deformable models represent curves or surfaces in the image domain that are warped by internal forces (which specify the regularity of the boundary surface) and external forces (which drive the surface to image features, usually intensity gradients) to produce a final segmentation. One such deformable model, called active contours or snakes, is a series of control points forming a 3D surface that is often initialised with *a priori* knowledge of the DGM anatomy and then driven towards image gradients in the target image, which has been used to segment the basal ganglia (Belitz et al., 2006). The attraction of the surface to these image gradients may be enhanced and using gradient vector flow, which has been used to achieve a segmentation of the thalamus and caudate (Colliot et al., 2006). Manually defined *a priori* rules based on the shape, size and location of each subcortical structure were used to produce fuzzy tissue maps in several studies (Zhou and Rajapakse, 2005), allowing the DGM to be revealed as the areas of GM adjacent to specific areas of the lateral ventricles (Barra and Boire, 2001). The Chan-Vese algorithm for active contours was used in one study, using a contour of the DGM generated from multiple training segmentations and driven by both attraction to image gradients and internal shape parameters, however was not found to outperform FIRST or FreeSurfer (Uzunbas et al., 2010). This class of techniques require additional MRI sequences to full resolve the boundary of the DGM to improve their performance, particularly for the anterior boundary of the thalamus which is not discernible from T1-weighted sequences.

### 3.3. Learning-based approaches

Image segmentation using deep learning approaches, most commonly Convolutional Neural Networks (CNNs), utilise a set of image data with associated ground truth labels to "learn" high-level image features associated with these labels, which are encoded in the model as a series of weights. An example of a CNN architecture used for image segmentation, called U-Net (Ronneberger et al., 2015), is illustrated in Fig. 6. Following this initial training of the model, the CNN can then infer these labels on new data, allowing segmentation of specific anatomies to be obtained. Early neural networks utilised manually segmented training sets in both 2D and 3D applications, and achieved a high reliability in DGM segmentation compared to manual ground truths (Magnotta et al., 1999). In another early neural network approach, spatial and intensity information is fused by a fuzzy multi-layer perceptron to achieve a segmentation of the DGM (Peng et al., 2005). Segmentations of the DGM have also been obtained using Artificial Neural Networks (ANNs) (Powell et al., 2008, 2006), as well as SVMs based on the CNN architecture (Powell et al., 2007), both of which utilise template-based segmentation for training. This later approach is included in the BRAINSCut software, which has been applied to a multicentre dataset to assess DGM segmentation (Kim et al., 2014).

The DGM has been segmented in multiple cohorts, including cohorts of neonates, young adults and ageing adults, using a CNN with both T1- and T2-weighted sequences as inputs, with the DSC ranging between 0.87 and 0.91 (Moeskops et al., 2016). Recent CNNs such as these utilise multiscale filters and several layers to isolate image features, however such an architecture typically contains millions of parameters, hence in this study segmentation was only performed on 2D images. Improved performance can be obtained using 3D CNN's, provided sufficient data is available to train such complex models without overfitting. A 3D CNN called DeepNAT, which uses both T1-weighted MRI as well as a spatial encoding using the Laplacian operator as inputs, and performs a spatial regularisation post-processing step using Conditional Random Fields

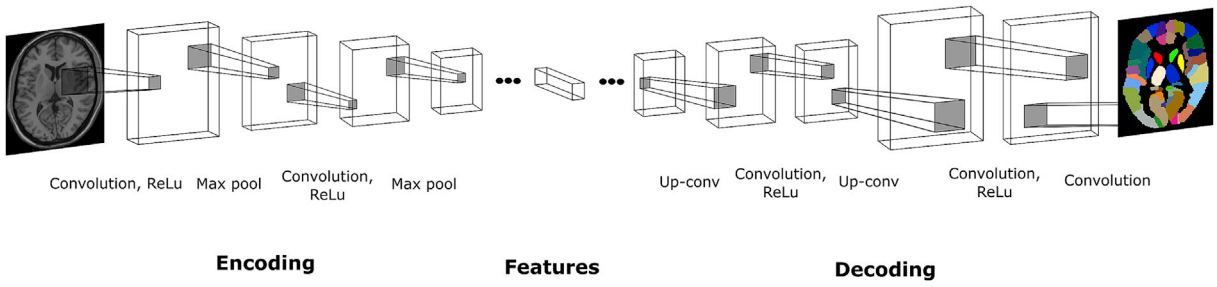


**Fig. 6.** Illustration of the U-Net CNN architecture (Ronneberger et al., 2015), outlining the steps involved in the encoding steps (including iterative convolutions and employing rectified linear unit (ReLu) activation function, and max-pooling operations) to obtain a feature vector, and then the decoding steps (iterated up-convolution and convolutions and ReLu) to obtain the final segmentation.

(CRF), achieved DSCs between 0.85 and 0.9 across all DGM structures (Wachinger et al., 2018). Similar DSC scores were achieved using another CNN, which used small kernels to facilitate deeper architectures, and combined global and local features (Dolz et al., 2016). In another approach, a 3D CNN was trained using T1-, T2-FLAIR and T1-Inversion Recovery sequences, allowing the segmentation of the DGM structures in patients with WM hyperintensities (Moeskops et al., 2018). Dictionary approaches are another form of learning-based algorithm that consist of model training and testing phases. In one study, a sparse, multiclass dictionary of image patches with their respective segmentation was learned, using an approach that enforces balance of all classes in the dictionary, which was then used for the segmentation of the DGM (Benkarim et al., 2017).

## 4. Software resources

The task of automatically obtaining DGM segmentations from MRIs has been facilitated by several freely available software packages. The range of free software available for this task are listed in Table 1 below. Such tools make the task of DGM segmentation available to all researchers, however obtain the segmentation using diverse approaches. All of the software packages utilise atlas *a priori* information to some extent, with some packages additionally using shape models and mesh deformations to refine the DGM segmentation. Although many CNN models for DGM segmentation exist, including existing architectures (such as U-Net and DeepNAT) and frameworks (such as TensorFlow), the under-representation of CNN-based software in this table may be due to the general nature of this approach. No CNN approach is specific to the task of DGM segmentation, but rather many CNN segmentations approaches can be used provided DGM labels exist on a training dataset.

FSL's FIRST (Patenaude et al., 2011) is one frequently used software for the task of DGM segmentation, which utilises a trained shape model of the DGM, represented as a 3D mesh. During model training, this DGM mesh has been iteratively deformed to segmentations in a training set whilst retaining measures of shape similarity to parametrise variation in DGM shape, with the simultaneous modelling of DGM intensities with Gaussian distributions incorporated using an AAM. For aligning this model to a target image, an initial affine registration into MNI space using FLIRT linear registration, followed by a second registration using only the region around the subcortical structures. Once aligned, the DGM shape model is then transformed along its learned eigenvectors to match image intensities and regularisations of shape using the Bayesian framework. The final mesh is then converted into a voxel segmentation and boundary correction is performed as a post-processing step. FIRST has been used for DGM segmentation in a wide variety of clinical applications, including AD (Cherubini et al., 2010; de Jong et al., 2008; Lee et al., 2017; Li et al., 2013; Möller et al., 2015; O'Dwyer et al., 2012; Štěpán-Buksakowska et al., 2014; Unay, 2012; Yi et al., 2016), PD (Acosta-Cabronero et al., 2017; Menke et al., 2014; Sunwoo et al., 2013), HD (van den Bogaard et al., 2013), post-traumatic stress disorder (Veer et al., 2015), schizophrenia (Spoletini et al., 2011), healthy controls (Hibar et al., 2015; Király et al., 2016; Péran et al., 2009; Rentería et al., 2014; T. Tang et al., 2013; Zhang et al., 2013), and most commonly in MS (Amann et al., 2015; Bishop et al., 2017; Chu et al., 2017; Dolezal et al., 2013; Eshaghi et al., 2018; Kim et al., 2017; Popescu et al., 2014; Shiee et al., 2012; Shinohara et al., 2017). In addition the SIENAX pipeline, which is an extended version of the SIENA software (Smith et al., 2002), includes DGM segmentation using FIRST, which has been used in one study for assessing DGM volumes in MS patients (Battaglini et al., 2018). Although SIENAX was observed to frequently misclassify the DGM as CSF when no prior probabilities were used (Lee and Prohovnik, 2008), when prior probabilities were provided it was observed to be in close agreement with SPM. The DGM segmentations obtained from FIRST have been refined in multiple studies using a mesh-based AAM that showed DGM volume reductions in patients with PD (Gazzina et al., 2016), whilst no changes in regional shape were observed in patients with tinnitus (Tae et al., 2018). The DGM segmentations from FIRST have facilitated several subsequent analyses of the DGM, such as VBM to assess regional DGM atrophy, as well as diffusion MR sequences to assess microstructural properties in these DGM regions, which identified atrophy and FA differences in patients with epilepsy (Peng et al., 2014). An improved FIRST pipeline has been developed, which additionally uses QSM maps with T1, and also incorporates non-linear registration, to further improve the accuracy of DGM segmentation (Feng et al., 2017). Both QSM and transverse relaxation rates (R2*) were used with DGM segmentations obtained from FIRST to identify differences in iron accumulation in MS patients and healthy controls (Elkady et al., 2017).

Although FreeSurfer focusses on surface-based analyses and cortical surface reconstruction using deformable 3D meshes (Fischl, 2012), it additionally performs segmentation of the DGM using an aligned probabilistic atlas and known intensity statistics and spatial relationships (observed from a training set) to compute a probability of DGM class

**Table 1**
Outline of freely available software for DGM segmentation from MRI.

| Software | Method | Website |
|---|---|---|
| BRAINSCut (Powell et al., 2008) | ANN | https://na-mic.org/wiki/BRAINSCut |
| FreeSurfer (Fischl, 2012) | Probabilistic atlas registration; Bayesian classification with MRF | https://surfer.nmr.mgh.harvard.edu/ |
| FSL FIRST (Patenaude et al., 2011) | PDM construction; linear and non-linear registration; AAM deformation | https://fsl.fmrib.ox.ac.uk/fsl/fslwiki/FIRST |
| LesionTOADS (Solomon et al., 2017) | Probabilistic atlas registration; fuzzy C-means clustering with outlier detection | https://www.nitrc.org/projects/toads-cruise/ |
| SPM (Penny et al., 2011) | Probabilistic atlas registration; GMM | http://www.fil.ion.ucl.ac.uk/spm/ |
| volBrain (Manjón and Coupé, 2016) | Multi-atlas registration; patch-based label fusion | http://volbrain.upv.es/ |

AAM, Active Appearance Models; ANN, Artificial Neural Networks; GMM, Gaussian Mixture Modelling; MRF, Markov Random Fields; PDM, Point Distribution Model; SPM, Statistical Parametric Mapping.

(Fischl et al., 2002). DGM segmentation using FreeSurfer has been used for investigating changes related to MS (Al-Radaideh et al., 2018; Galego et al., 2015; Krämer et al., 2015; Ramasamy et al., 2009), AD (Cui et al., 2012; Lehmann et al., 2010; Oliveira et al., 2010; Westman et al., 2012), PD (Bilgic et al., 2012; Choi et al., 2015; Lee et al., 2017; Messina et al., 2011; Tinaz et al., 2011; Vasconcellos et al., 2018; Wang et al., 2018), schizophrenia (Bollettini et al., 2018; Goldman et al., 2008; Juuhl--Langseth et al., 2012; Rich et al., 2016; van Erp et al., 2016; Vaskinn et al., 2015), bipolar disorder (Abramovic et al., 2016; Arumugham et al., 2017; Sacchet et al., 2015), HD (Majid et al., 2011; Rupp et al., 2012), temporal lobe epilepsy (Alhusaini et al., 2013; McDonald et al., 2008), human immunodeficiency virus (Corrêa et al., 2016b, 2016a), traumatic brain injury (Hellstrøm et al., 2017), paediatric brain injury (Bigler et al., 2010) and healthy controls (Dennison et al., 2013; Grazioplene et al., 2015; Kang et al., 2015; Kremen et al., 2010; Liem et al., 2015; Long et al., 2012; Ostby et al., 2009; Potvin et al., 2016; Winkelmann et al., 2016). Test-retest data on healthy participants showed FreeSurfer had a high reliability for DGM segmentations despite varying pulse sequence (Wonderlick et al., 2009). FreeSurfer has been used to segment the DGM on sub-millimetre gradient-echo MRIs, with improved resolutions of subcortical structures yielding consistent segmentations (Wu et al., 2010). In another study, FreeSurfer was combined with magnetic resonance elastography to investigate viscoelastic mechanical properties of the DGM (Johnson et al., 2016).

The SPM software performs tissue segmentation using the EM algorithm with affinely aligned tissue probability maps (Ashburner and Friston, 1997). Whilst SPM can perform segmentations of the three brain tissues (CSF, GM and WM), it can perform DGM segmentation using several atlases with subcortical labels, such as the Harvard-Oxford subcortical structural atlas (Brandão and Bastos-Leite, 2016), the North Carolina neonatal atlas (Donald et al., 2016) and the Individual Brain Atlases using Statistical Parametric Mapping Software (IBASPM) (Clark et al., 2012). IBASPM was found to provide less accurate segmentations of the DGM compared to FreeSurfer, relative to a manual labelling (Dewey et al., 2010). DGM volumes can also be obtained using the VBM8 toolbox in SPM with several modifications, including Hidden Markov Fields, spatial DGM priors, diffeomorphic registration algorithm (DARTEL) registration and adaptive non-local means noise removal, which was also shown to be comparable to FreeSurfer (Grimm et al., 2015). Additional MR sequences have been used to isolate the DGM from the overall GM segmentation using SPM. For instance magnetisation transfer (MT) sequences, which are based on the R1 and R2*, were used to provide an improved segmentation of the DGM compared to MPRAGE, when using SPM (Callaghan et al., 2016; Helms et al., 2009). Additionally, the MANTiS toolbox for SPM utilises the SPM segmentation as well as a 40 week infant template to perform neonatal DGM segmentation (Beare et al., 2016), which was used to reveal significantly reduced volumes compared to term-born controls (Loh et al., 2017).

Another software package called LesionTOADS software uses both T1- and T2-weighted MRI to the DGM structures as well as WM lesions, which was used to reveal thalamus volume being significantly smaller in MS patients (Solomon et al., 2017), and was shown to have high a scan-rescan reliability for the DGM on a cohort of 21 healthy participants (Landman et al., 2013). LesionTOADS was found to be more impacted by site location, with site being found to be associated with 96% of variation in thalamus volume in one patient with recurring MS, when compared to FIRST (84%) (Shinohara et al., 2017). However the potential advantage of LesionTOADS, is that it also identifies WM lesions prevalent in MS, which has been shown to artificially impact measures of DGM volume obtained from FIRST in one study (Gelineau-Morel et al., 2012), although in another study WM lesions were not found to impact DGM volume from FIRST (Popescu et al., 2014). The NeuroQuant software package (CorTechs Labs, La Jolla, California) is another automated approach used for DGM segmentation, which was used to find significantly reduced amygdala and caudate volumes in patients with psychotic disorders (Eggins et al., 2018). The performance of NeuroQuant was compared to FreeSurfer on a cohort of patients with mild traumatic brain injury, and showed that while both methods showed excellent reliability, both produced different anatomical volumes from each other (Reid et al., 2017). An automated online tool called volBrain is a multi-atlas patch-based label fusion segmentation method that utilises manual segmentations of the DGM and a weighted label voting scheme incorporating patch spatial and intensity similarity (Manjón and Coupé, 2016). One study quantified subcortical volume changes across brain maturation using volBrain, and found decreases in GM volume for all structures except the amygdala (Coupé et al., 2017). In another study, volBrain was found to perform similarly to a multi-atlas approach that used T1 and QSM sequences, and slightly outperformed FIRST for all subcortical structures except the globus pallidus (Li et al., 2019).

With the wide range of available software for the task of DGM segmentation, several studies have assessed the comparative performance of these software packages. In a comparison between FIRST, FreeSurfer, SIENAX and Multispectral Bayesian Classifier (MBC) with six manual expert segmentations showed that FIRST and FreeSurfer produced relatively more accurate segmentations of the DGM (Derakhshan et al., 2010), owing to the specific DGM focus of these two packages. However findings comparing FreeSurfer and FIRST are mixed, with some studies reporting FIRST had higher scan-rescan reliability than FreeSurfer across time points on a large dataset ($n = 235$) (Guadalupe et al., 2014), improved agreement with manual ground truth segmentation particularly for the putamen (Perlaki et al., 2017) and improved DGM segmentation in patients with MS lesions (González-Villà et al., 2017). In contrast, several studies instead show FreeSurfer to have the greater scan-rescan reliability across all subcortical structures (Morey et al., 2010), increased reliability in measuring longitudinal changes in patients with Alzheimer's diseases (Meijerman et al., 2018) and slightly improved agreement with manual ground truth segmentations and stereological measurements on a large dataset ($n = 281$) (Akudjedu et al., 2018) compared to FIRST, and other studies have reported an almost perfect agreement between the two packages (Vidal-Jordana et al., 2017). The potentially improved performance of FIRST has resulted in some studies using FIRST for DGM segmentation and FreeSurfer instead for cortical GM segmentation (Herranz et al., 2016). Among the studies included in this review, the average DGM volume of studies using FIRST was 0.82, compared to 0.77 for FreeSurfer. Improved DGM segmentation accuracy for both FIRST and FreeSurfer was achieved using an approach to enhance WM/GM tissue contrast using T1- and T2-weighted MRI sequences (Misaki et al., 2015).

Studies comparing multi-atlas based approaches with the existing software packages have typically shown atlas fusion to yield an improved DGM segmentation. Multi-atlas label fusion approach was found to yield the best performance compared to an atlas and EM-based segmentation, an active appearance model, and a Bayesian appearance model (Babalola et al., 2009; Kolawole O. Babalola et al., 2008). Compared to a gold standard segmentation, MAGeT was found to agree most with manual segmentations, while both FreeSurfer and FIRST overestimated DGM volumes, with FreeSurfer performing better on the thalamus and FIRST performing better on the pallidus (Makowski et al., 2018). Another atlas fusion algorithm called local MAP PSTAPLE obtained the most reliable subcortical volumes when compared to both FreeSurfer and FIRST (Velasco-Annis et al., 2018).

## 5. Applications of DGM segmentation

### 5.1. Volumetry

The main clinical application of DGM segmentation is to measure subcortical volume, which can reflect potential atrophy of these structures. For instance, AD is associated with cortical and deep GM atrophy and ventricular enlargement, and among many of the reviewed studies reduced DGM volume has been consistently observed (Cherubini et al., 2010; de Jong et al., 2008; Lee et al., 2017; Li et al., 2013; Möller et al.,

2015; Štěpán-Buksakowska et al., 2014; Yi et al., 2016), a finding supported in a cohort with ventriculomegaly (Scott et al., 2013). Similarly in MS, which is characterised by demyelinating WM lesions but is also associated with GM atrophy (Fisher et al., 2008), reduced DGM volumes were consistently found among reviewed studies (Bishop et al., 2017; Fujiwara et al., 2017; Kim et al., 2017; Ramasamy et al., 2009; Shiee et al., 2012; Solomon et al., 2017), with only one study reporting no volume decline in patients with MS (Dolezal et al., 2013). Other populations where reductions in DGM volume were consistently observed include preterm/very preterm infants (Juuhl-Langseth et al., 2012; Loh et al., 2017; Makropoulos et al., 2016), as well as patients with traumatic brain injury (Hellstrøm et al., 2017; Zagorchev et al., 2016) and psychiatric or depressive disorders (Dombrovski et al., 2012; Eggins et al., 2018; Harrisberger et al., 2016; Lu et al., 2016). Although Parkinson's disease is known to be associated with dysfunction of the DGM (Marsden and Obeso, 1994), this may not present as a reduction in DGM volume. Although several of the reviewed studies found a reduction in PD patients (Bilgic et al., 2012; Lee et al., 2017; Mak et al., 2014; Sunwoo et al., 2013), others found no volume change (Acosta and Pearl, 2004; Choi et al., 2015; Messina et al., 2011; Tinaz et al., 2011). In addition, many studies have found that DGM volumes vary both with age as well as gender (Coupé et al., 2017; Király et al., 2018; Raznahan et al., 2014; Sussman et al., 2016; Tang et al., 2013). Accounting for these age and gender related differences, DGM volumetry could potentially be used to classify such neurological disease from healthy controls, and in some cases could even estimate severity of disease symptoms (Lu et al., 2016).

Several reviewed studies have focussed on the segmentation on subthalamic nuclei, which have largely been achieved with multi-atlas approaches, such as the MAGeT approach (Magon et al., 2015) or the big data registration enhancement approach utilising over five thousand atlases (Bao et al., 2019). Due to the heterogenous appearance of these nuclei, increased anatomical contrast can be achieved by acquiring additional MRI sequences, such as T2* (Xiao et al., 2017) and QSM (Zhang et al., 2018). Both these studies generate new atlases for the task of subthalamic segmentation, which are important in order to target certain regions with deep brain stimulation, a common therapy for patients with PD (Kleiner-Fisman et al., 2006).

### 5.2. Diffusion tractography

Accurate segmentations of the DGM play an important role in diffusion MRI as they can be used as a Region of Interest (ROI) to seed tractography as in several reviewed studies (Barron et al., 2014; Corrêa et al., 2017, 2016b), however the microstructural information can be used to further refine the DGM segmentation (Peng et al., 2014; Visser et al., 2016). Probabilistic tractography was performed in one study using the FMRIB's Diffusion Toolbox to create a probability distribution function of fibre orientations around the thalamus, which was then used to refine the segmentation of the thalamus, which is not discernible from structural MRI alone (Elias et al., 2012). As the thalamus has three major WM radiations emanating from it in different directions, the segmentation of the sub-thalamic nuclei also been achieved in several studies using diffusion tensor imaging (DTI) along with a structural atlas to segment the individual regions of the thalamus (Mang et al., 2012; Stough et al., 2013; Unrath et al., 2008). In one atlas-based approach T1, T2, proton density and diffusion sequences were incorporated to perform segmentation of individual thalamic nuclei (Ewert et al., 2018). Sub-thalamic segmentation was also achieved using diffusion MRI in one study following FreeSurfer delineation of the DGM (Battistella et al., 2017). While diffusion tractography, along with the iron-sensitive R2* and QSM sequences, has demonstrated benefit for the segmentation subthalamic nuclei using the thalamic radiations, the applicability of DGM segmentations in diffusion tractography presents a wider opportunity to probe the microstructural integrity of WM radiations emanating from the DGM.

### 5.3. Textural analysis

Once segmentations of the DGM have been obtained, various methods for texture analyses can be performed to quantify possible DGM injury, and can be used for disease diagnosis. For instance, after manual segmentation of the DGM, textural analysis of these anatomies from T1 images revealed textural features to be approximately 68% accurate in classifying patients with Amyotrophic Lateral Sclerosis (ALS) and healthy controls (de Albuquerque et al., 2016). In another study utilising manual segmentations of the putamen which were co-registered to a standard putamen model shape, textural features from T1-, T2-weighted and proton density sequences in the putamen were characterised, which were found to be associated with the diagnosis of Creutzfeldt-Jakob disease (CJD) (Bouyagoub et al., 2014). Both of these studies use the MaZda software package to perform MRI texture analysis (Szczypiński et al., 2009), which extract three categories of texture features: statistical features based on the image histogram, model features using generative or stochastic approaches, and transform features such as Gabor, Fourier or wavelet transforms. Using manual segmentations of the putamen, intensity gradients of T2- and proton density MR sequences revealed to be diagnostically important for the diagnosis of Creutzfeldt-Jakob disease (Hojjat et al., 2002). However, while textural features of the DGM have been found to be indicative of some diseases, ALS and CJD specifically, textural information is currently being used only as a post-processing step, and not yet been demonstrated as beneficial for DGM segmentation.

### 5.4. Shape modelling

Once segmentations of the DGM have been obtained, several shape modelling approaches have also been used to compare shape differences between two cohorts. For example, following an atlas-based segmentation of the DGM using the MaGeT algorithm, a surface-based method of quantifying anatomical shape (Lerch et al., 2008) was performed to quantify subthalamic structure and volume displacements relative to the template shape model in MS patients (Magon et al., 2014). In a similar vertex-based shape approach on patients with psychiatric disorders, amygdala volume was found to be associated with causal awareness (Griffiths et al., 2016), whilst a vertex-wise analysis on patients with ALS revealed changes in the thalamus and caudate nucleus (Bede et al., 2013). In several studies, following DGM segmentations using FIRST, volumetric segmentations were converted to a 3D mesh, and then a vertex-wise statistical analysis of the aligned 3D meshes was performed revealing significant shape differences in the caudate, nucleus accumbens and pallidum on patients with HIV (Kuhn et al., 2017), regional shrinkage in the anterior thalamus in patients with AD (Štěpán-Buksakowska et al., 2014), volume loss in the putamen and caudate in patients with HD (van den Bogaard et al., 2011), and no regional differences in patients with PD (Mak et al., 2014). Following manual segmentation of the putamen, a similar mesh alignment was achieved fluid registration and tensor based morphometry, which revealed local shape differences in premature neonates compared to term born controls (Shi et al., 2012). Anatomical mesh modelling of the caudate and putamen, which were previously segmented using deformable registration, revealed local atrophy in a cohort of patients with HIV (Becker et al., 2011). Using semi-automated segmentations of the DGM, multi-object Procrustes alignment followed by distance-weighted discrimination of shape using SVM, differences in shape between children with autism spectrum disorder (ASD) and healthy controls were observed (Gorczowski et al., 2010). These methods for comparing DGM shape between two groups remain valuable in the research setting to improve understanding of brain function and in the impact of pathology. However, the limitation of these analyses is that the vertex-wise correspondence across several meshes remains a challenging task, and in cases where some of the anatomy may be missing due to injury, the 'true' correspondence is not known.

### 5.5. Voxel based morphometry

Voxel-based approaches such as VBM (Ashburner and Friston, 2000) perform a statistical test across each aligned voxel across the series of images, and relies on an accurate alignment of multiple MRIs. Such an approach allows DGM volume to be ascertained relative to a control group, as the statistical tests capture the relative difference in DGM intensity. Therefore voxel-based methods do not perform a traditional segmentation of the DGM *i.e.* a 3D ROI of the anatomy, but rather reflect voxel-wise changes in tissue volume or density between two sets of images (Good et al., 2001), which may be in the DGM. For instance, a VBM analysis revealed significant atrophy in the DGM, particularly the caudate and thalamus, in patients with AD (Karas et al., 2003). Such analyses still require an accurate alignment of the images so that the statistics compare similar anatomy, which is often performed using DARTEL (Ashburner, 2007). Additionally, many studies perform tissue segmentation prior to VBM to spatially localise the analysis to reduce the number of statistical tests performed. In patients with paediatric MS, VBM analysis following a local threshold segmentation of the DGM revealed reduced thalamus volume compared to controls (Mesaros et al., 2008). In another study, following segmentation with the SPM software (Penny et al., 2011), VBM revealed volume differences in the DGM of patients with MS, and additionally observed different MS sub-groups using SVM (Bendfeldt et al., 2012). VBM has revealed GM loss in the globus pallidus and thalamus associated with the progression of HD (Douaud et al., 2006), and has identified GM atrophy occurring during healthy aging (Peelle et al., 2012). Although MPRAGE is typically used for VBM analyses, other sequences can be used. For instance tissue probability maps (TPMs) of the DGM were constructed using R2* MRIs aligned in the MNI space using DARTEL and using VBM on the R2* values in the DGM revealed age related decreased in DGM volume (Lorio et al., 2016). While VBM can estimate atrophy through voxel-wise intensity differences, the necessity of an accurate voxel-wise alignment remains challenging in many cohorts with brain injury, and would be impacted by the presence of WM lesions iso-intense with the DGM. In this way, 3D segmentations, which are contextually aware of the surrounding neighbourhood, may be best the best approach for accurately estimating the atrophy of these structures.

## 6. Discussion

### 6.1. Summary of methods

The main methods presented in the reviewed studies, including atlas-based, algorithmic-based and learning-based approaches, all have different strengths and limitations in the task of DGM segmentation. Atlas-based methods, for instance, can achieve an accurate segmentation through one or more sets of ground truth *a priori* labels, and additionally benefit from ease of atlas construction with no model training being necessary. Accommodating a greater anatomical variability can be achieved in numerous ways, including using multiple different atlases, flexible long-distance registration approaches, and weighted label fusion strategies. However these approaches critically rely on an accurate segmentation between the target image and the atlas, hence extreme deviations in anatomy as well as brain injuries may not be well aligned to, and hence segmented by, the atlas. Furthermore atlas approaches may be computationally expensive, particularly with multiple atlases necessitating multiple registrations to the target.

It is this limitation of atlas methods that algorithm-based methods may help alleviate. Whilst the term algorithm-based approaches could include any of the reviewed methods, in this review refers specifically to the group of approaches that are primarily driven by image intensity and shape information, which unlike atlas methods can adapt to specific cases of variability anatomy or extreme injury. Additionally, these methods typically are easy to implement and are relatively computationally efficient. However as these approaches are based by image information, they are also more prone to processes that corrupt this information, including image noise and MR artefacts, and also may get caught more easily on local-minima.

Finally learning-based approaches achieved the best overall DGM segmentation accuracy (average DSC = 0.856) compared to the other approaches, which can be bolstered by the depth and heterogeneity of the training set of images, and is robust to image noise and artefacts. Like algorithmic-methods, learning-approaches require training, however this learning phase is more important for learning-based approaches which are more prone to overfitting and consequently reduced segmentation performance on new datasets. Additionally, 3D CNNs are computationally expensive to train, require hyperparameter tuning to achieve optimal performance, and the resulting models may be obscure and difficult to interpret effectively.

### 6.2. Addressing the challenges of DGM segmentation

To summarise, the current challenges for DGM segmentation include low contrast on the boundary of the structures and the presence of WM lesions isointense to the DGM which can complicate algorithmic methods, high anatomical variability and injury heterogeneity which may complicate atlas-based methods, and the limited ground truth training data needed to construct accurate and generalisable deep learning models. In this section, we will outline the current approaches best suited for addressing these individual challenges.

One prevalent issue with DGM segmentation is the lack of contrast of parts of the subcortical structures from T1 sequences. One strategy for overcoming this is the right selection of MR sequences, with at least a T1-weighted sequence being necessary due to its wide availability and standardised sequences. Still, care should be taken choosing T1-weighted sequences for DGM segmentation, as it was shown that the DGM probability maps were significantly larger in MP2RAGE compared to MPRAGE (Okubo et al., 2016). Studies should aim to utilise 3T scanning to leverage the improved image resolution to better quantify the ground truth structure. For instance using the FIRST pipeline, it was found that 3T imaging provided superior differentiation of the DGM, and improved scan-rescan repeatability compared to 1.5T imaging (Chu et al., 2017). In addition to T1, including R2*/T2*/QSM sequences which leverage the increased iron concentration of the DGM may better resolve these structures than T1 imaging alone. The benefit of incorporating these sequences has been shown with an increased performance in multi-atlas approaches (Fujiwara et al., 2017; Li et al., 2019), as well as its inclusion in the FIRST pipeline (Feng et al., 2017). However the iron concentration measured by these sequences has been shown to have an age-related effect, leading to an apparent loss in GM volume with age (Lorio et al., 2014), and also changes based on pathology, with atrophy appearing as abnormal iron deposition typical of neurodegeneration (Lorio et al., 2016). Another limitation to including such sequences is the additional scanning time (approximately 5 min) (Cercignani et al., 2005), but this can be overcame by additionally acquiring phase information from a T1 echo-based sequence, such as MP2RAGE, to obtain the R2*. One final limitation for building models dependent on these sequences as an input is their limited availability, particularly in comparison to standardised T1 sequences. Future studies should endeavour to acquire R2*/T2*/QSM sequences, either as an input to enhance segmentation pipelines, or to generate an "improved" ground truth DGM segmentation to train deep learning models. In this way, CNN models will remain widely applicable due to requiring only the T1 sequence, whilst still benefitting from the improved contrast from the magnetisation transfer sequences via the modified ground truth.

One of the biggest challenges for DGM segmentation is the variability in anatomy, both in terms of healthy anatomical variability and changes caused by brain injury. Many techniques are currently equipped to address healthy anatomical variability, particularly multi-atlas approaches, such as MAGeT (Chakravarty et al., 2006), which can further be improved in accuracy using symmetric registrations (Tao et al., 2009). Propagating labels across targets, creating new labelled atlases and

dividing large differences in anatomy to several smaller registrations are alternate strategies for effectively addressing potential variability (Sullivan et al., 2011). Furthermore modified atlas selection and label weighting approaches have been proposed, such as atlas selection based on NMI (Wu et al., 2007), weighted label voting based on similarity (Wang et al., 2014) and L3 label fusion (Weisenfeld and Warfield, 2011), to better segment target anatomy using the most similar existing structure and labels. Accommodating severe brain injury is more challenging as it covers significantly more variation in brain structure which cannot feasibly be modelled *a priori*. For instance, in MRIs of patients with normal pressure hydrocephalus, the enlarged ventricles required manual tracing in addition to using FIRST to accommodate the potential displacement of the DGM. As severe tissue loss may lead to an altered orientation of the brain and the DGM within the head, an improved alignment can be made with highly elastic registrations such as LDDMM (Beg et al., 2005; Khan et al., 2008), or alternatively two stages of registration can be performed, one global and one local as in FIRST (Patenaude et al., 2011). Furthermore as brain injury and tissue loss leads to CSF filling the space, registration guided by intensity information could prove to be robust to this injury (Meier and Fisher, 2005), or can be guided by the lateral ventricles adjacent to the DGM which similarly can be enlarged due to injury (Linguraru et al., 2006). Alternatively, following an initial registration, subsequent methods driven by image forces can be used to fit injury not seen on existing templates, such as EM-driven mesh deformation (Puonti et al., 2013), EM-driven atlas deformation (Lotjonen et al., 2009; Tang et al., 2013) and EM-MRF following multi-atlas registration (Makropoulos et al., 2014). Level sets have also been proposed as a post-processing step for accurately refining segmentations based on intensity information (Metzger et al., 2016; Raviv et al., 2009; Riklin-Raviv et al., 2010), which may prove robust to tissue loss. Therefore, to accommodate severe injury, studies could adopt a tailored registration approach to fit the altered DGM position, or include post-processing steps to refine the segmentation in case that part of DGM tissue is missing and replaced by CSF.

SSMs have traditionally been used for DGM segmentation, which benefit from the relative convexity in DGM shape, and can model variations in healthy anatomy through the encoded through eigenmodes learned from a representative training set. Indeed this approach is used by FIRST (Patenaude et al., 2011), which was the best performing of the freely-available software in similarity to ground truth (González-Villà et al., 2017; Perlaki et al., 2017) and scan-rescan reliability (Guadalupe et al., 2014). This approach has been further advanced with improved boundary detection (Wenzel et al., 2018) and multi-scale shape fitting (Cerrolaza et al., 2015). However the limitation of shape models is that, whilst able to accurately capture variations in healthy anatomical variability, capturing the increased variability in DGM shape caused by potential injury would be significantly more difficult. Segmenting DGM structures impacted by injury using SSMs trained on healthy data may be less suitable as variations in DGM shape caused by brain injury may not be captured by the "healthy" eigenmodes. AAMs may help alleviate this issue (Babalola et al., 2008), as the captured variations in image texture from a healthy dataset may help refine the shape model based on the significantly differing intensities in the target image. Alternatively, training SSMs using examples of injured DGM would require a lot of training examples to capture the range of variability in injury, and also impact the segmentation of healthy DGM due to the eigenmodes representing combinations of both "healthy" and "injured" shapes.

Associated with brain injury and pathology is the potential presence of brain lesions, typically in the WM, which may impact the segmentation of the DGM. As such the segmentation of the lesions beforehand is necessary, and can be achieved with several software packages such as LesionTOADS or the Lesion Segmentation Toolbox (LST) in SPM. As WM lesions can be isointense with the DGM, both software packages require a T2-weighted sequence such as FLAIR which can better visualise periventricular lesions (Tan et al., 2002). Future studies should include lesion segmentation approaches, either interleaved with lesion segmentation derived from the same *a priori* tissue information (Datta and Narayana, 2013), or prior to DGM segmentation using the available approaches, particularly for cohorts of patients where WM lesions are common, such as MS. Furthermore these automated lesion segmentation tools can generate lesion labels on a training dataset for CNNs (Moeskops et al., 2018), as has been demonstrated in several studies on combined brain tissue and lesion segmentation (Li et al., 2018; Narayana et al., 2018).

The advent of deep learning has provided new opportunities for image segmentation using convolutional networks to learn high level features. Indeed, such approaches have shown the highest average agreement with manual ground truth segmentations of the DGM, which will only improve as larger datasets with increased anatomical and pathological variability become available. Architectures such as DeepNAT further improve accuracy by including spatial information as an input as well as CRF post-processing (Wachinger et al., 2018), and utilising multi-scale patches to classify based on global and local features (Dolz et al., 2016). However deep learning has its limitations, namely that it can overfit on limited datasets, necessitating large well-annotated data to produce generalisable models, and often requiring transfer learning for pre-trained networks to perform accurately on new datasets (Shin et al., 2016). The availability of multiple large-scale datasets across multiple domains (such as the ADNI dataset for AD (Petersen et al., 2010), the ABIDE dataset for autism (Di Martino et al., 2014), and the Healthy Brain Network (HBN) healthy pediatric dataset (Alexander et al., 2017) ) may help to minimise this issue, however not all datasets have an annotated ground truth and so other automated methods may have to be employed to build a sufficient training set for deep learning. Advancement of deep learning approaches will require an established "silver standard" approach to generate a large-scale annotated training dataset, for instance with multi-atlas approaches which have shown second best the performance to date outside of deep learning. Overcoming scarcity and variability in data are critical for training generalisable deep learning models, which may be achieved with data augmentation strategies, including diffeomorphic warping, patch-based reflections and rotations, and changing image contrast and resolutions (Perez and Wang, 2017), and transfer-learning from different datasets, which has been shown to produce similar segmentation accuracy with reduced training images and faster training speed (Kushibar et al., 2019).

## 7. Conclusion

The automated segmentation of the subcortical structures has clinical utility in quantifying atrophy and estimating patient diagnosis and prognosis, however is limited by several technical challenges, particularly in cohorts with neurological conditions. Approaches that utilised registered atlases, methods driven by image and shape features and learning-based approaches were reviewed, as well as freely available software packages. In the comparison of these different methods, deep learning approaches were found to achieve the best overall performance, with multi-atlas approaches achieving the second highest performance. Furthermore FSL's FIRST showed the highest reported segmentation performance among the available software packages. To address the technical challenges in segmenting the subcortical structures in various cohorts with potential brain injury, several recommendations are suggested. Specifically for limited contrast of the DGM from structural sequences, future studies could additionally acquire R2* sequences either to improve intensity-driven algorithms with the clear DGM boundary provided by these sequences, or to improve ground truth segmentations for annotated training datasets used for deep learning. Lesion segmentation should also be performed in addition to the DGM for certain cohorts, in order to extract iso-intense lesions which could impact subcortical segmentation. Achieving robustness to varying anatomy and potentially severe brain injury may best be achieved with multi-atlas approaches, leveraging multiple channels and highly elastic transformations where possible, and followed by intensity-driven post-processing steps to refine the segmentations based on potential tissue loss.

Alternatively deep learning approaches could be used, leveraging freely available datasets, with multi-atlas approaches providing a "silver standard" annotated dataset for model training. With such advancements, accurate DGM segmentation could be achieved in all patients, regardless of neurological condition. This would allow MR quantification to provide clinically useful information to healthcare professionals, which can help to tailor patient-specific treatment and improve functional outcomes for patients with neurological conditions.

## Acknowledgements

Alex M. Pagnozzi is supported by the Advance Queensland Research Fellowship (AQR16816-17RD2). This funding body has not contributed to the study design, the collection, management, analysis and interpretation of data, the writing of final reports or the decision to submit findings for publication. No other authors have potential conflicts of interest to declare.

## Appendix A. Supplementary data

Supplementary data to this article can be found online at https://doi.org/10.1016/j.neuroimage.2019.116018.

## References

Hibar, D.P., Stein, J.L., Renteria, M.E., Arias-Vasquez, A., Desrivières, S., Jahanshad, N., Toro, R., Wittfeld, K., Abramovic, L., Andersson, M., Aribisala, B.S., Armstrong, N.J., Bernard, M., Bohlken, M.M., Boks, M.P., Bralten, J., Brown, A.A., Mallar Chakravarty, M., Chen, Q., Ching, C.R.K., Cuellar-Partida, G., den Braber, A., Giddaluru, S., Goldman, A.L., Grimm, O., Guadalupe, T., Hass, J., Woldehawariat, G., Holmes, A.J., Hoogman, M., Janowitz, D., Jia, T., Kim, S., Klein, M., Kraemer, B., Lee, P.H., Olde Loohuis, L.M., Luciano, M., Macare, C., Mather, K.A., Mattheisen, M., Milaneschi, Y., Nho, K., Papmeyer, M., Ramasamy, A., Risacher, S.L., Roiz-Santiañez, R., Rose, E.J., Salami, A., Sämann, P.G., Schmaal, L., Schork, A.J., Shin, J., Strike, L.T., Teumer, A., van Donkelaar, M.M.J., van Eijk, K.R., Walters, R.K., Westlye, L.T., Whelan, C.D., Winkler, A.M., Zwiers, M.P., Alhusaini, S., Athanasiu, L., Ehrlich, S., Hakobjan, M.M.H., Hartberg, C.B., Haukvik, U.K., Heister, A.J.G.A.M., Hoehn, D., Kasperaviciute, D., Liewald, D.C.M., Lopez, L.M., Makkinje, R.R.R., Matarin, M., Naber, M.A.M., Reese McKay, D., Needham, M., Nugent, A.C., Pütz, B., Royle, N.A., Shen, L., Sprooten, E., Trabzuni, D., van der Marel, S.S.L., van Hulzen, K.J.E., Walton, E., Wolf, C., Almasy, L., Ames, D., Arepalli, S., Assareh, A.A., Bastin, M.E., Brodaty, H., Bulayeva, K.B., Carless, M.A., Cichon, S., Corvin, A., Curran, J.E., Czisch, M., de Zubicaray, G.I., Dillman, A., Duggirala, R., Dyer, T.D., Erk, S., Fedko, I.O., Ferrucci, L., Foroud, T.M., Fox, P.T., Fukunaga, M., Raphael Gibbs, J., Göring, H.H.H., Green, R.C., Guelfi, S., Hansell, N.K., Hartman, C.A., Hegenscheid, K., Heinz, A., Hernandez, D.G., Heslenfeld, D.J., Hoekstra, P.J., Holsboer, F., Homuth, G., Hottenga, J.-J., Ikeda, M., Jack, C.R., Jenkinson, M., Johnson, R., Kanai, R., Keil, M., Kent, J.W., Kochunov, P., Kwok, J.B., Lawrie, S.M., Liu, X., Longo, D.L., McMahon, K.L., Meisenzahl, E., Melle, I., Mohnke, S., Montgomery, G.W., Mostert, J.C., Mühleisen, T.W., Nalls, M.A., Nichols, T.E., Nilsson, L.G., Nöthen, M.M., Ohi, K., Olvera, R.L., Perez-Iglesias, R., Bruce Pike, G., Potkin, S.G., Reinvang, I., Reppermund, S., Rietschel, M., Romanczuk-Seiferth, N., Rosen, G.D., Rujescu, D., Schnell, K., Schofield, P.R., Smith, C., Steen, V.M., Sussmann, J.E., Thalamuthu, A., Toga, A.W., Traynor, B.J., Troncoso, J., Turner, J.A., Valdés Hernández, M.C., van 't Ent, D., van der Brug, M., van der Wee, N.J.A., van Tol, M.-J., Veltman, D.J., Wassink, T.H., Westman, E., Zielke, R.H., Zonderman, A.B., Ashbrook, D.G., Hager, R., Lu, L., McMahon, F.J., Morris, D.W., Williams, R.W., Brunner, H.G., Buckner, R.L., Buitelaar, J.K., Cahn, W., Calhoun, V.D., Cavalleri, G.L., Crespo-Facorro, B., Dale, A.M., Davies, G.E., Delanty, N., Depondt, C., Djurovic, S., Drevets, W.C., Espeseth, T., Gollub, R.L., Ho, B.-C., Hoffmann, W., Hosten, N., Kahn, R.S., Le Hellard, S., Meyer-Lindenberg, A., Müller-Myhsok, B., Nauck, M., Nyberg, L., Pandolfo, M., Penninx, B.W.J.H., Roffman, J.L., Sisodiya, S.M., Smoller, J.W., van Bokhoven, H., van Haren, N.E.M., Völzke, H., Walter, H., Weiner, M.W., Wen, W., White, T., Agartz, I., Andreassen, O.A., Blangero, J., Boomsma, D.I., Brouwer, R.M., Cannon, D.M., Cookson, M.R., de Geus, E.J.C., Deary, I.J., Donohoe, G., Fernández, G., Fisher, S.E., Francks, C., Glahn, D.C., Grabe, H.J., Gruber, O., Hardy, J., Hashimoto, R., Hulshoff Pol, H.E., Jönsson, E.G., Kloszewska, I., Lovestone, S., Mattay, V.S., Mecocci, P., McDonald, C., McIntosh, A.M., Ophoff, R.A., Paus, T., Pausova, Z., Ryten, M., Sachdev, P.S., Saykin, A.J., Simmons, A., Singleton, A., Soininen, H., Wardlaw, J.M., Weale, M.E., Weinberger, D.R., Adams, H.H.H., Launer, L.J., Seiler, S., Schmidt, R., Chauhan, G., Satizabal, C.L., Becker, J.T., Yanek, L., van der Lee, S.J., Ebling, M., Fischl, B., Longstreth, W.T., Greve, D., Schmidt, H., Nyquist, P., Vinke, L.N., van Duijn, C.M., Xue, L., Mazoyer, B., Bis, J.C., Gudnason, V., Seshadri, S., Ikram, M.A., Martin, N.G., Wright, M.J., Schumann, G., Franke, B., Thompson, P.M., Medland, S.E., Wright, M.J., Schumann, G., Franke, B., Thompson, P.M., Medland, S.E., 2015. Common genetic variants influence human subcortical brain structures. Nature 520, 224–229. https://doi.org/10.1038/nature14101.

van Erp, T.G.M., Hibar, D.P., Rasmussen, J.M., Glahn, D.C., Pearlson, G.D., Andreassen, O.A., Agartz, I., Westlye, L.T., Haukvik, U.K., Dale, A.M., Melle, I., Hartberg, C.B., Gruber, O., Kraemer, B., Zilles, D., Donohoe, G., Kelly, S., McDonald, C., Morris, D.W., Cannon, D.M., Corvin, A., Machielsen, M.W.J., Koenders, L., de Haan, L., Veltman, D.J., Satterthwaite, T.D., Wolf, D.H., Gur, R.C., Gur, R.E., Potkin, S.G., Mathalon, D.H., Mueller, B.A., Preda, A., Macciardi, F., Ehrlich, S., Walton, E., Hass, J., Calhoun, V.D., Bockholt, H.J., Sponheim, S.R., Shoemaker, J.M., van Haren, N.E.M., Pol, H.E.H., Ophoff, R.A., Kahn, R.S., Roiz-Santiañez, R., Crespo-Facorro, B., Wang, L., Alpert, K.I., Jönsson, E.G., Dimitrova, R., Bois, C., Whalley, H.C., McIntosh, A.M., Lawrie, S.M., Hashimoto, R., Thompson, P.M., Turner, J.A., 2016. Subcortical brain volume abnormalities in 2028 individuals with schizophrenia and 2540 healthy controls via the ENIGMA consortium. Mol. Psychiatry 21, 547–553. https://doi.org/10.1038/mp.2015.63.

Abramovic, L., Boks, M.P.M., Vreeker, A., Bouter, D.C., Kruiper, C., Verkooijen, S., van Bergen, A.H., Ophoff, R.A., Kahn, R.S., van Haren, N.E.M., 2016. The association of antipsychotic medication and lithium with brain measures in patients with bipolar disorder. Eur. Neuropsychopharmacol. 26, 1741–1751. https://doi.org/10.1016/j.euroneuro.2016.09.371.

Acosta, M.T., Pearl, P.L., 2004. Imaging data in autism: from structure to malfunction. Semin. Pediatr. Neurol. 11, 205–213. https://doi.org/10.1016/j.spen.2004.07.004.

Acosta-Cabronero, J., Cardenas-Blanco, A., Betts, M.J., Butryn, M., Valdes-Herrera, J.P., Galazky, I., Nestor, P.J., 2017. The whole-brain pattern of magnetic susceptibility perturbations in Parkinson's disease. Brain 140, 118–131. https://doi.org/10.1093/brain/aww278.

Akhondi Asl, A., Soltanian-Zadeh, H., 2008. Constrained optimization of nonparametric entropy-based segmentation of brain structures. In: 2008 5th IEEE International Symposium on Biomedical Imaging: from Nano to Macro. IEEE, pp. 41–44. https://doi.org/10.1109/ISBI.2008.4540927.

Akhondi-Asl, A., Soltanian-Zadeh, H., 2010. Two-stage multishape segmentation of brain structures using image intensity, tissue type, and location informationa). Med. Phys. 37, 4501–4516. https://doi.org/10.1118/1.3459018.

Akhoundi-Asl, A., Soltanian-Zadeh, H., 2007. NONPARAMETRIC ENTROPY-BASED COUPLED MULTI-SHAPE MEDICAL IMAGE SEGMENTATION. In: 2007 4th IEEE International Symposium on Biomedical Imaging: from Nano to Macro. IEEE, pp. 1200–1203. https://doi.org/10.1109/ISBI.2007.357073.

Akudjedu, T.N., Nabulsi, L., Makelyte, M., Scanlon, C., Hehir, S., Casey, H., Ambati, S., Kenney, J., O'Donoghue, S., McDermott, E., Kilmartin, L., Dockery, P., McDonald, C., Hallahan, B., Cannon, D.M., 2018. A comparative study of segmentation techniques for the quantification of brain subcortical volume. Brain Imag. Behav. 12, 1678–1695. https://doi.org/10.1007/s11682-018-9835-y.

Al-Radaideh, A., Athamneh, I., Alabadi, H., Hbahbih, M., 2018. Cortical and subcortical morphometric and iron changes in relapsing-remitting multiple sclerosis and their association with white matter T2 lesion load. Clin. Neuroradiol. https://doi.org/10.1007/s00062-017-0654-0.

Alexander, L.M., Escalera, J., Ai, L., Andreotti, C., Febre, K., Mangone, A., Vega-Potler, N., Langer, N., Alexander, A., Kovacs, M., Litke, S., 2017. An open resource for transdiagnostic research in pediatric mental health and learning disorders. Scientific data 4, 170181.

Alhusaini, S., Scanlon, C., Ronan, L., Maguire, S., Meaney, J.F., Fagan, A.J., Boyle, G., Borgulya, G., Iyer, P.M., Brennan, P., Costello, D., Chaila, E., Fitzsimons, M., Doherty, C.P., Delanty, N., Cavalleri, G.L., 2013. Heritability of subcortical volumetric traits in mesial temporal lobe epilepsy. PLoS One 8, e61880. https://doi.org/10.1371/journal.pone.0061880.

Amann, M., Andělová, M., Pfister, A., Mueller-Lenke, N., Traud, S., Reinhardt, J., Magon, S., Bendfeldt, K., Kappos, L., Radue, E.-W., Stippich, C., Sprenger, T., 2015. Subcortical brain segmentation of two dimensional T1-weighted data sets with FMRIB's Integrated Registration and Segmentation Tool (FIRST). NeuroImage Clin. 7, 43–52. https://doi.org/10.1016/j.nicl.2014.11.010.

Aquino, D., Bizzi, A., Grisoli, M., Garavaglia, B., Bruzzone, M.G., Nardocci, N., Savoiardo, M., Chiapparini, L., 2009. Age-related iron deposition in the basal ganglia: quantitative analysis in healthy subjects. Radiology 252, 165–172. https://doi.org/10.1148/radiol.2522081399.

Aravamuthan, B.R., Waugh, J.L., 2016. Localization of basal ganglia and thalamic damage in dyskinetic cerebral palsy. Pediatr. Neurol. 54, 11–21. https://doi.org/10.1016/J.PEDIATRNEUROL.2015.10.005.

Arumugham, S.S., Torres, I.J., Lang, D.J., Su, W., Lam, R.W., Honer, W.G., Yatham, L.N., 2017. Subcortical structural volumes in recently remitted first episode mania. J. Affect. Disord. 222, 23–27. https://doi.org/10.1016/j.jad.2017.06.051.

Ashburner, J., 2007. A fast diffeomorphic image registration algorithm. Neuroimage 38, 95–113. https://doi.org/10.1016/j.neuroimage.2007.07.007.

Ashburner, J., Friston, K., 1997. Multimodal image coregistration and partitioning—a unified framework. Neuroimage 6, 209–217. https://doi.org/10.1006/nimg.1997.0290.

Ashburner, J., Friston, K.J., 2000. Voxel-based morphometry — the methods. Neuroimage 821, 805–821. https://doi.org/10.1006/nimg.2000.0582.

Babalola, K., Cootes, T., 2010. Using parts and geometry models to initialise Active Appearance Models for automated segmentation of 3D medical images. In: 2010 IEEE International Symposium on Biomedical Imaging: from Nano to Macro. IEEE, pp. 1069–1072. https://doi.org/10.1109/ISBI.2010.5490177.

Babalola, K.O., Cootes, T.F., Twining, C.J., Petrovic, V., Taylor, C.J., 2008. 3D brain segmentation using active appearance models and local regressors. Med. Image Comput. Comput. Assist. Interv. 11, 401–408.

Babalola, Kolawole O., Patenaude, B., Aljabar, P., Schnabel, J., Kennedy, D., Crum, W., Smith, S., Cootes, T.F., Jenkinson, M., Rueckert, D., 2008. Comparison and Evaluation of Segmentation Techniques for Subcortical Structures in Brain MRI.

Springer, Berlin, Heidelberg, pp. 409–416. https://doi.org/10.1007/978-3-540-85988-8_49.
Babalola, K.O., Patenaude, B., Aljabar, P., Schnabel, J., Kennedy, D., Crum, W., Smith, S., Cootes, T., Jenkinson, M., Rueckert, D., 2009. An evaluation of four automatic methods of segmenting the subcortical structures in the brain. Neuroimage 47, 1435–1447. https://doi.org/10.1016/j.neuroimage.2009.05.029.
Babikian, V.L., Wolfe, N., Linn, R., Knoefel, J.E., Albert, M.L., Michel, J.-P., Bouras, C., Giannakopoulos, P., 1990. Cognitive changes in patients with multiple cerebral infarcts. Stroke 21, 1013–1018. https://doi.org/10.1161/01.str.23.9.1225.
Bao, S., Bermudez, C., Huo, Y., Parvathaneni, P., Rodriguez, W., Resnick, S.M., D'Haese, P.-F., McHugo, M., Heckers, S., Dawant, B.M., Lyu, I., Landman, B.A., 2019. Registration-based image enhancement improves multi-atlas segmentation of the thalamic nuclei and hippocampal subfields. Magn. Reson. Imaging 59, 143–152. https://doi.org/10.1016/J.MRI.2019.03.014.
Barra, V., Boire, J.-Y., 2001. Automatic segmentation of subcortical brain structures in MR images using information fusion. IEEE Trans. Med. Imaging 20, 549–558. https://doi.org/10.1109/42.932740.
Barron, D.S., Tandon, N., Lancaster, J.L., Fox, P.T., 2014. Thalamic structural connectivity in medial temporal lobe epilepsy. Epilepsia 55 e50–e55. https://doi.org/10.1111/epi.12637.
Battaglini, M., Jenkinson, M., De Stefano, N., Alzheimer's Disease Neuroimaging Initiative, 2018. SIENA-XL for improving the assessment of gray and white matter volume changes on brain MRI. Hum. Brain Mapp. 39, 1063–1077. https://doi.org/10.1002/hbm.23828.
Battistella, G., Najdenovska, E., Maeder, P., Ghazaleh, N., Daducci, A., Thiran, J.-P., Jacquemont, S., Tuleasca, C., Levivier, M., Bach Cuadra, M., Fornari, E., 2017. Robust thalamic nuclei segmentation method based on local diffusion magnetic resonance properties. Brain Struct. Funct. 222, 2203–2216. https://doi.org/10.1007/s00429-016-1336-4.
Beare, R.J., Chen, J., Kelly, C.E., Alexopoulos, D., Smyser, C.D., Rogers, C.E., Loh, W.Y., Matthews, L.G., Cheong, J.L.Y., Spittle, A.J., Anderson, P.J., Doyle, L.W., Inder, T.E., Seal, M.L., Thompson, D.K., 2016. Neonatal brain tissue classification with morphological adaptation and unified segmentation. Front. Neuroinform. 10, 12. https://doi.org/10.3389/fninf.2016.00012.
Becker, J.T., Sanders, J., Madsen, S.K., Ragin, A., Kingsley, L., Maruca, V., Cohen, B., Goodkin, K., Martin, E., Miller, E.N., Sacktor, N., Alger, J.R., Barker, P.B., Saharan, P., Carmichael, O.T., Thompson, P.M., Multicenter AIDS Cohort Study, M.A.C., 2011. Subcortical brain atrophy persists even in HAART-regulated HIV disease. Brain Imag. Behav. 5, 77–85. https://doi.org/10.1007/s11682-011-9113-8.
Bede, P., Elamin, M., Byrne, S., McLaughlin, R.L., Kenna, K., Vajda, A., Pender, N., Bradley, D.G., Hardiman, O., 2013. Basal ganglia involvement in amyotrophic lateral sclerosis. Neurology 81, 2107–2115. https://doi.org/10.1212/01.wnl.0000437313.80913.2c.
Beg, M.F., Miller, M.I., Trouvé, A., Younes, L., 2005. Computing large deformation metric mappings via geodesic flows of diffeomorphisms. Int. J. Comput. Vis. 61, 139–157. https://doi.org/10.1023/B:VISI.0000043755.93987.aa.
Belitz, H., Rohr, K., Muller, H., Wagenknecht, G., 2006. First results of an automated model-based segmentation system for subcortical structures in human brain MRI data. In: 3rd IEEE International Symposium on Biomedical Imaging: Macro to Nano, 2006. IEEE, pp. 402–405. https://doi.org/10.1109/ISBI.2006.1624938.
Bendfeldt, K., Klöppel, S., Nichols, T.E., Smieskova, R., Kuster, P., Traud, S., Mueller-Lenke, N., Naegelin, Y., Kappos, L., Radue, E.-W., Borgwardt, S.J., 2012. Multivariate pattern classification of gray matter pathology in multiple sclerosis. Neuroimage 60, 400–408. https://doi.org/10.1016/J.NEUROIMAGE.2011.12.070.
Benedict, R.H.B., Ramasamy, D., Munschauer, F., Weinstock-Guttman, B., Zivadinov, R., 2009. Memory impairment in multiple sclerosis: correlation with deep grey matter and mesial temporal atrophy. J. Neurol. Neurosurg. Psychiatry 80, 201–206. https://doi.org/10.1136/jnnp.2008.148403.
Benkarim, O.M., Piella, G., González Ballester, M.A., Sanroma, G., Alzheimer's Disease Neuroimaging Initiative, 2017. Discriminative confidence estimation for probabilistic multi-atlas label fusion. Med. Image Anal. 42, 274–287. https://doi.org/10.1016/j.media.2017.08.008.
Bigler, E.D., Abildskov, T.J., Wilde, E.A., McCauley, S.R., Li, X., Merkley, T.L., Fearing, M.A., Newsome, M.R., Scheibel, R.S., Hunter, J.V., Chu, Z., Levin, H.S., 2010. Diffuse damage in pediatric traumatic brain injury: a comparison of automated versus operator-controlled quantification methods. Neuroimage 50, 1017–1026. https://doi.org/10.1016/j.neuroimage.2010.01.003.
Bilgic, B., Bayram, A., Arslan, A.B., Hanagasi, H., Dursun, B., Gurvit, H., Emre, M., Lohmann, E., 2012. Differentiating symptomatic Parkin mutations carriers from patients with idiopathic Parkinson's disease: contribution of automated segmentation neuroimaging method. Park. Relat. Disord. 18, 562–566. https://doi.org/10.1016/j.parkreldis.2012.02.017.
Bishop, C.A., Newbould, R.D., Lee, J.S., Honeyfield, L., Quest, R., Colasanti, A., Ali, R., Mattoscio, M., Cortese, A., Nicholas, R., Matthews, P.M., Muraro, P.A., Waldman, A.D., 2017. Analysis of ageing-associated grey matter volume in patients with multiple sclerosis shows excess atrophy in subcortical regions. NeuroImage Clin. 13, 9–15. https://doi.org/10.1016/j.nicl.2016.11.005.
Boardman, J.P., Counsell, S.J., Rueckert, D., Kapellou, O., Bhatia, K.K., Aljabar, P., Hajnal, J., Allsop, J.M., Rutherford, M.A., Edwards, A.D., 2006. Abnormal deep grey matter development following preterm birth detected using deformation-based morphometry. Neuroimage 32, 70–78. https://doi.org/10.1016/J.NEUROIMAGE.2006.03.029.
Boecker, H., Jankowski, J., Ditter, P., Scheef, L., 2008. A role of the basal ganglia and midbrain nuclei for initiation of motor sequences. Neuroimage 39, 1356–1369. https://doi.org/10.1016/J.NEUROIMAGE.2007.09.069.
Bollettini, I., Spangaro, M., Poletti, S., Lorenzi, C., Pirovano, A., Vai, B., Smeraldi, E., Cavallaro, R., Benedetti, F., 2018. Sexually divergent effect of COMT Val/met genotype on subcortical volumes in schizophrenia. Brain Imag. Behav. 12, 829–836. https://doi.org/10.1007/s11682-017-9748-1.
Bouyagoub, S., Cimpan, I.C., Hojjatoleslami, S.A., Kume, A., Mah, Y.H., Colchester, A.C.F., 2014. Modelling Smooth Intensity Changes in the Putamen for Diagnosis of Sporadic Creutzfeldt-Jakob Disease. Springer, Cham, pp. 134–142. https://doi.org/10.1007/978-3-319-05666-1_17.
Brandão, S., Bastos-Leite, A.J., 2016. Magnetisation-prepared rapid gradient-echo versus inversion recovery turbo spin-echo T1-weighted images for segmentation of deep grey matter structures at 3 T. Clin. Radiol. 71, 1304–1308. https://doi.org/10.1016/j.crad.2016.09.009.
Brieman, L., Breiman, L., Brieman, L., Breiman, L., 2001. Random Forests. Mach. Learn. 45, 5–32. https://doi.org/10.1023/A:1010933404324.
Callaghan, M.F., Mohammadi, S., Weiskopf, N., 2016. Synthetic quantitative MRI through relaxometry modelling. NMR Biomed. 29, 1729–1738. https://doi.org/10.1002/nbm.3658.
Cercignani, M., Symms, M.R., Schmierer, K., Boulby, P.A., Tozer, D.J., Ron, M., Tofts, P.S., Barker, G.J., 2005. Three-dimensional quantitative magnetisation transfer imaging of the human brain. Neuroimage 27, 436–441. https://doi.org/10.1016/J.NEUROIMAGE.2005.04.031.
Cerrolaza, J.J., Villanueva, A., Cabeza, R., 2012. Hierarchical statistical shape models of multiobject anatomical structures: application to brain MRI. IEEE Trans. Med. Imaging 31, 713–724. https://doi.org/10.1109/TMI.2011.2175940.
Cerrolaza, J.J., Reyes, M., Summers, R.M., González-Ballester, M.Á., Linguraru, M.G., 2015. Automatic multi-resolution shape modeling of multi-organ structures. Med. Image Anal. 25, 11–21. https://doi.org/10.1016/j.media.2015.04.003.
Chakravarty, M.M., Bertrand, G., Hodge, C.P., Sadikot, A.F., Collins, D.L., 2006. The creation of a brain atlas for image guided neurosurgery using serial histological data. Neuroimage 30, 359–376. https://doi.org/10.1016/j.neuroimage.2005.09.041.
Chakravarty, M.M., Sadikot, A.F., Germann, J., Bertrand, G., Collins, D.L., 2008. Towards a validation of atlas warping techniques. Med. Image Anal. 12, 713–726. https://doi.org/10.1016/j.media.2008.04.003.
Chakravarty, M.M., Sadikot, A.F., Germann, J., Hellier, P., Bertrand, G., Collins, D.L., 2009. Comparison of piece-wise linear, linear, and nonlinear atlas-to-patient warping techniques: analysis of the labeling of subcortical nuclei for functional neurosurgical applications. Hum. Brain Mapp. 30, 3574–3595. https://doi.org/10.1002/hbm.20780.
Chakravarty, M.M., Steadman, P., van Eede, M.C., Calcott, R.D., Gu, V., Shaw, P., Raznahan, A., Collins, D.L., Lerch, J.P., 2013. Performing label-fusion-based segmentation using multiple automatically generated templates. Hum. Brain Mapp. 34, 2635–2654. https://doi.org/10.1002/hbm.22092.
Cherubini, A., Péran, P., Spoletini, I., Di Paola, M., Di Iulio, F., Hagberg, G.E., Sancesario, G., Gianni, W., Bossù, P., Caltagirone, C., Sabatini, U., Spalletta, G., 2010. Combined volumetry and DTI in subcortical structures of mild cognitive impairment and Alzheimer's disease patients. J. Alzheimer's Dis. 19, 1273–1282. https://doi.org/10.3233/JAD-2010-091186.
Choi, S.-M., Kim, B.C., Chang, J., Choi, K.-H., Nam, T.-S., Kim, J.-T., Lee, S.-H., Park, M.-S., Yoon, W., de Leon, M.J., 2015. Comparison of the brain volume in essential tremor and Parkinson's disease tremor using an automated segmentation method. Eur. Neurol. 73, 303–309. https://doi.org/10.1159/000381708.
Chu, R., Hurwitz, S., Tauhid, S., Bakshi, R., 2017. Automated segmentation of cerebral deep gray matter from MRI scans: effect of field strength on sensitivity and reliability. BMC Neurol. 17, 172. https://doi.org/10.1186/s12883-017-0949-4.
Clark, U.S., Cohen, R.A., Sweet, L.H., Gongvatana, A., Devlin, K.N., Hana, G.N., Westbrook, M.L., Mulligan, R.C., Jerskey, B.A., White, T.L., Navia, B., Tashima, K.T., 2012. Effects of HIV and early life stress on amygdala morphometry and neurocognitive function. J. Int. Neuropsychol. Soc. 18, 657–668. https://doi.org/10.1017/S1355617712000434.
Cobzas, D., Sun, H., Walsh, A.J., Lebel, R.M., Blevins, G., Wilman, A.H., 2015. Subcortical gray matter segmentation and voxel-based analysis using transverse relaxation and quantitative susceptibility mapping with application to multiple sclerosis. J. Magn. Reson. Imaging 42, 1601–1610. https://doi.org/10.1002/jmri.24951.
Colliot, O., Camara, O., Bloch, I., 2006. Integration of fuzzy spatial relations in deformable models—application to brain MRI segmentation. Pattern Recognit. 39, 1401–1414. https://doi.org/10.1016/J.PATCOG.2006.02.022.
Cook, D., Kesner, R.P., 1988. Caudate nucleus and memory for egocentric localization. Behav. Neural. Biol. 49, 332–343. https://doi.org/10.1016/S0163-1047(88)90338-X.
Cools, R., Clark, L., Owen, A.M., Robbins, T.W., 2002. Defining the neural mechanisms of probabilistic reversal learning using event-related functional magnetic resonance imaging. J. Neurosci. 22, 4563–4567. https://doi.org/10.1523/JNEUROSCI.22-11-04563.2002.
Corrêa, D.G., Zimmermann, N., Netto, T.M., Tukamoto, G., Ventura, N., de Castro Bellini Leite, S., Cabral, R.F., Fonseca, R.P., Bahia, P.R.V., Gasparetto, E.L., 2016a. Regional cerebral gray matter volume in HIV-positive patients with executive function deficits. J. Neuroimaging 26, 450–457. https://doi.org/10.1111/jon.12327.
Corrêa, D.G., Zimmermann, N., Tukamoto, G., Doring, T., Ventura, N., Leite, S.C.B., Cabral, R.F., Fonseca, R.P., Bahia, P.R.V., Gasparetto, E.L., 2016b. Longitudinal assessment of subcortical gray matter volume, cortical thickness, and white matter integrity in HIV-positive patients. J. Magn. Reson. Imaging 44, 1262–1269. https://doi.org/10.1002/jmri.25263.
Corrêa, D.G., Ventura, N., Zimmermann, N., Doring, T.M., Tukamoto, G., Leme, J., Pereira, M., D'Andrea, I., Rêgo, C., Alves-Leon, S.V., Gasparetto, E.L., 2017. Evaluation of deep gray matter volume, cortical thickness and white matter integrity

in patients with typical absence epilepsy: a study using voxelwise-based techniques. Neuroradiology 59, 237–245. https://doi.org/10.1007/s00234-017-1782-6.
Cortes, C., Vapnik, V., 1995. Support-vector networks. Mach. Learn. 20, 273–297.
Coupé, P., Catheline, G., Lanuza, E., Manjón, J.V., Alzheimer's Disease Neuroimaging Initiative, 2017. Towards a unified analysis of brain maturation and aging across the entire lifespan: a MRI analysis. Hum. Brain Mapp. 38, 5501–5518. https://doi.org/10.1002/hbm.23743.
Cui, Y., Wen, W., Lipnicki, D.M., Beg, M.F., Jin, J.S., Luo, S., Zhu, W., Kochan, N.A., Reppermund, S., Zhuang, L., Raamana, P.R., Liu, T., Trollor, J.N., Wang, L., Brodaty, H., Sachdev, P.S., 2012. Automated detection of amnestic mild cognitive impairment in community-dwelling elderly adults: a combined spatial atrophy and white matter alteration approach. Neuroimage 59, 1209–1217. https://doi.org/10.1016/j.neuroimage.2011.08.013.
Datta, S., Narayana, P.A., 2013. A comprehensive approach to the segmentation of multichannel three-dimensional MR brain images in multiple sclerosis. NeuroImage. Clin. 2, 184–196. https://doi.org/10.1016/j.nicl.2012.12.007.
de Albuquerque, M., Anjos, L.G.V., Maia Tavares de Andrade, H., de Oliveira, M.S., Castellano, G., Junqueira Ribeiro de Rezende, T., Nucci, A., Cavalcante França Junior, M., 2016. MRI texture analysis reveals deep gray nuclei damage in amyotrophic lateral sclerosis. J. Neuroimaging 26, 201–206. https://doi.org/10.1111/jon.12262.
de Jong, L.W., van der Hiele, K., Veer, I.M., Houwing, J.J., Westendorp, R.G.J., Bollen, E.L.E.M., de Bruin, P.W., Middelkoop, H.A.M., van Buchem, M.A., van der Grond, J., 2008. Strongly reduced volumes of putamen and thalamus in Alzheimer's disease: an MRI study. Brain 131, 3277–3285. https://doi.org/10.1093/brain/awn278.
de Jong, L.W., Vidal, J.-S., Forsberg, L.E., Zijdenbos, A.P., Haight, T., Sigurdsson, S., Gudnason, V., van Buchem, M.A., Launer, L.J., 2017. Allometric scaling of brain regions to intra-cranial volume: an epidemiological MRI study. Hum. Brain Mapp. 38, 151–164. https://doi.org/10.1002/hbm.23351.
Dempster, A.P., Laird, N.M., Rubin, D.B., 1977. Maximum likelihood from incomplete data via the EM algorithm. J. R. Stat. Soc. Ser. B 39, 1–38.
Dennison, M., Whittle, S., Yücel, M., Vijayakumar, N., Kline, A., Simmons, J., Allen, N.B., 2013. Mapping subcortical brain maturation during adolescence: evidence of hemisphere- and sex-specific longitudinal changes. Dev. Sci. 16, 772–791. https://doi.org/10.1111/desc.12057.
Derakhshan, M., Caramanos, Z., Giacomini, P.S., Narayanan, S., Maranzano, J., Francis, S.J., Arnold, D.L., Collins, D.L., 2010. Evaluation of automated techniques for the quantification of grey matter atrophy in patients with multiple sclerosis. Neuroimage 52, 1261–1267. https://doi.org/10.1016/j.neuroimage.2010.05.029.
Dewey, J., Hana, G., Russell, T., Price, J., McCaffrey, D., Harezlak, J., Sem, E., Anyanwu, J.C., Guttmann, C.R., Navia, B., Cohen, R., Tate, D.F., HIV Neuroimaging Consortium, 2010. Reliability and validity of MRI-based automated volumetry software relative to auto-assisted manual measurement of subcortical structures in HIV-infected patients from a multisite study. Neuroimage 51, 1334–1344. https://doi.org/10.1016/j.neuroimage.2010.03.033.
Di Martino, A., Yan, C.-G., Li, Q., Denio, E., Castellanos, F.X., Alaerts, K., Anderson, J.S., Assaf, M., Bookheimer, S.Y., Dapretto, M., Deen, B., Delmonte, S., Dinstein, I., Ertl-Wagner, B., Fair, D.A., Gallagher, L., Kennedy, D.P., Keown, C.L., Keysers, C., Lainhart, J.E., Lord, C., Luna, B., Menon, V., Minshew, N.J., Monk, C.S., Mueller, S., Müller, R.-A., Nebel, M.B., Nigg, J.T., O'Hearn, K., Pelphrey, K.A., Peltier, S.J., Rudie, J.D., Sunaert, S., Thioux, M., Tyszka, J.M., Uddin, L.Q., Verhoeven, J.S., Wenderoth, N., Wiggins, J.L., Mostofsky, S.H., Milham, M.P., 2014. The autism brain imaging data exchange: towards a large-scale evaluation of the intrinsic brain architecture in autism. Mol. Psychiatry 19, 659–667. https://doi.org/10.1038/mp.2013.78.
Djamanakova, A., Faria, A.V., Hsu, J., Ceritoglu, C., Oishi, K., Miller, M.I., Hillis, A.E., Mori, S., 2013. Diffeomorphic brain mapping based on T1-weighted images: improvement of registration accuracy by multichannel mapping. J. Magn. Reson. Imaging 37, 76–84. https://doi.org/10.1002/jmri.23790.
Dolezal, O., Gabelic, T., Horakova, D., Bergsland, N., Dwyer, M.G., Seidl, Z., Krasensky, J., Ramasamy, D.P., Vaneckova, M., Havrdova, E., Zivadinov, R., 2013. Development of gray matter atrophy in relapsing–remitting multiple sclerosis is not gender dependent: results of a 5-year follow-up study. Clin. Neurol. Neurosurg. 115, S42–S48. https://doi.org/10.1016/j.clineuro.2013.09.020.
Dolz, J., Massoptier, L., Vermandel, M., 2015. Segmentation algorithms of subcortical brain structures on MRI for radiotherapy and radiosurgery: a survey. IRBM 36, 200–212. https://doi.org/10.1016/J.IRBM.2015.06.001.
Dolz, J., Desrosiers, C., Ayed, I. Ben, 2016. 3D fully convolutional networks for subcortical segmentation in MRI: A large-scale study. https://doi.org/10.1016/j.neuroimage.2017.04.039.
Dombrovski, A.Y., Siegle, G.J., Szanto, K., Clark, L., Reynolds, C.F., Aizenstein, H., 2012. The temptation of suicide: striatal gray matter, discounting of delayed rewards, and suicide attempts in late-life depression. Psychol. Med. 42, 1203–1215. https://doi.org/10.1017/S0033291711002133.
Donald, K.A., Fouche, J.P., Roos, A., Koen, N., Howells, F.M., Riley, E.P., Woods, R.P., Zar, H.J., Narr, K.L., Stein, D.J., 2016. Alcohol exposure in utero is associated with decreased gray matter volume in neonates. Metab. Brain Dis. 31, 81–91. https://doi.org/10.1007/s11011-015-9771-0.
Douaud, G., Gaura, V., Ribeiro, M.-J., Lethimonnier, F., Maroy, R., Verny, C., Krystkowiak, P., Damier, P., Bachoud-Levi, A.-C., Hantraye, P., Remy, P., 2006. Distribution of grey matter atrophy in Huntington's disease patients: a combined ROI-based and voxel-based morphometric study. Neuroimage 32, 1562–1575.
Eggins, P.S., Hatton, S.N., Hermens, D.F., Hickie, I.B., Lagopoulos, J., 2018. Subcortical volumetric differences between clinical stages of young people with affective and psychotic disorders. Psychiatry Res. Neuroimaging 271, 8–16. https://doi.org/10.1016/j.pscychresns.2017.11.015.
Eickhoff, S., Walters, N.B., Schleicher, A., Kril, J., Egan, G.F., Zilles, K., Watson, J.D.G., Amunts, K., 2005. High-resolution MRI reflects myeloarchitecture and cytoarchitecture of human cerebral cortex. Hum. Brain Mapp. 24, 206–215. https://doi.org/10.1002/hbm.20082.
Elias, W.J., Zheng, Z.A., Domer, P., Quigg, M., Pouratian, N., 2012. Validation of connectivity-based thalamic segmentation with direct electrophysiologic recordings from human sensory thalamus. Neuroimage 59, 2025–2034. https://doi.org/10.1016/j.neuroimage.2011.10.049.
Elkady, A.M., Cobzas, D., Sun, H., Blevins, G., Wilman, A.H., 2017. Progressive iron accumulation across multiple sclerosis phenotypes revealed by sparse classification of deep gray matter. J. Magn. Reson. Imaging 46, 1464–1473. https://doi.org/10.1002/jmri.25682.
Eshaghi, A., Prados, F., Brownlee, W.J., Altmann, D.R., Tur, C., Cardoso, M.J., De Angelis, F., van de Pavert, S.H., Cawley, N., De Stefano, N., Stromillo, M.L., Battaglini, M., Ruggieri, S., Gasperini, C., Filippi, M., Rocca, M.A., Rovira, A., Sastre-Garriga, J., Vrenken, H., Leurs, C.E., Killestein, J., Pirpamer, L., Enzinger, C., Ourselin, S., Wheeler-Kingshott, C.A.M.G., Chard, D., Thompson, A.J., Alexander, D.C., Barkhof, F., Ciccarelli, O., MAGNIMS study group, on behalf of the M. study, 2018. Deep gray matter volume loss drives disability worsening in multiple sclerosis. Ann. Neurol. 83, 210–222. https://doi.org/10.1002/ana.25145.
Ewert, S., Plettig, P., Li, N., Chakravarty, M.M., Collins, D.L., Herrington, T.M., Kühn, A.A., Horn, A., 2018. Toward defining deep brain stimulation targets in MNI space: a subcortical atlas based on multimodal MRI, histology and structural connectivity. Neuroimage 170, 271–282. https://doi.org/10.1016/j.neuroimage.2017.05.015.
Ewert, S., Horn, A., Finkel, F., Li, N., Kühn, A.A., Herrington, T.M., 2019. Optimization and comparative evaluation of nonlinear deformation algorithms for atlas-based segmentation of DBS target nuclei. Neuroimage 184, 586–598. https://doi.org/10.1016/J.NEUROIMAGE.2018.09.061.
Feng, X., Deistung, A., Dwyer, M.G., Hagemeier, J., Polak, P., Lebenberg, J., Frouin, F., Zivadinov, R., Reichenbach, J.R., Schweser, F., 2017. An improved FSL-FIRST pipeline for subcortical gray matter segmentation to study abnormal brain anatomy using quantitative susceptibility mapping (QSM). Magn. Reson. Imaging 39, 110–122. https://doi.org/10.1016/j.mri.2017.02.002.
Fischl, B., 2012. FreeSurfer. Neuroimage 62, 774–781. https://doi.org/10.1016/j.neuroimage.2012.01.021.
Fischl, B., Salat, D.H., Busa, E., Albert, M., Dieterich, M., Haselgrove, C., van der Kouwe, A., Killiany, R., Kennedy, D., Klaveness, S., Montillo, A., Makris, N., Rosen, B., Dale, A.M., 2002. Whole brain segmentation: automated labeling of neuroanatomical structures in the human brain. Neuron 33, 341–355.
Fisher, E., Lee, J.-C., Nakamura, K., Rudick, R.A., 2008. Gray matter atrophy in multiple sclerosis: a longitudinal study. Ann. Neurol. 64, 255–265. https://doi.org/10.1002/ana.21436.
Fujiwara, E., Kmech, J.A., Cobzas, D., Sun, H., Seres, P., Blevins, G., Wilman, A.H., 2017. Cognitive implications of deep gray matter iron in multiple sclerosis. Am. J. Neuroradiol. 38, 942–948. https://doi.org/10.3174/ajnr.A5109.
Galego, O., Gouveia, A., Batista, S., Moura, C., Machado, E., 2015. Brain atrophy and physical disability in primary progressive multiple sclerosis: a volumetric study. Neuroradiol. J. 28, 354–358. https://doi.org/10.1177/1971400915594984.
Garg, A., Appel-Cresswell, S., Popuri, K., McKeown, M.J., Beg, M.F., 2015. Morphological alterations in the caudate, putamen, pallidum, and thalamus in Parkinson's disease. Front. Neurosci. 9, 101. https://doi.org/10.3389/fnins.2015.00101.
Gazzina, S., Premi, E., Turrone, R., Acosta-Cabronero, J., Rizzetti, M.C., Cotelli, M.S., Gasparotti, R., Padovani, A., Borroni, B., 2016. Subcortical matter in the α-synucleinopathies spectrum: an MRI pilot study. J. Neurol. 263, 1575–1582. https://doi.org/10.1007/s00415-016-8173-5.
Gelineau-Morel, R., Tomassini, V., Jenkinson, M., Johansen-Berg, H., Matthews, P.M., Palace, J., 2012. The effect of hypointense white matter lesions on automated gray matter segmentation in multiple sclerosis. Hum. Brain Mapp. 33, 2802–2814. https://doi.org/10.1002/hbm.21402.
Goldman, A.L., Pezawas, L., Mattay, V.S., Fischl, B., Verchinski, B.A., Zoltick, B., Weinberger, D.R., Meyer-Lindenberg, A., 2008. Heritability of brain morphology related to schizophrenia: a large-scale Automated magnetic resonance imaging segmentation study. Biol. Psychiatry 63, 475–483. https://doi.org/10.1016/j.biopsych.2007.06.006.
González-Villà, S., Valverde, S., Cabezas, M., Pareto, D., Vilanova, J.C., Ramió-Torrentà, L., Rovira, À., Oliver, A., Lladó, X., 2017. Evaluating the effect of multiple sclerosis lesions on automatic brain structure segmentation. NeuroImage Clin. 15, 228–238. https://doi.org/10.1016/j.nicl.2017.05.003.
Good, C.D., Johnsrude, I.S., Ashburner, J., Henson, R.N.A., Friston, K.J., Frackowiak, R.S.J., 2001. A voxel-based morphometric study of ageing in 465 normal adult human brains. Neuroimage 14, 21–36. https://doi.org/10.1006/NIMG.2001.0786.
Gorczowski, K., Styner, M., Jeong, Ja Yeon, Marron, J.S., Piven, J., Hazlett, H.C., Pizer, S.M., Gerig, G., 2010. Multi-object analysis of volume, pose, and shape using statistical discrimination. IEEE Trans. Pattern Anal. Mach. Intell. 32, 652–661. https://doi.org/10.1109/TPAMI.2009.92.
Gorthi, S., 2016. Evaluation of the effect of doubling atlases using midsagittal plane on multi-atlas based segmentation of brain structures. In: 2016 38th Annual International Conference of the IEEE Engineering in Medicine and Biology Society (EMBC). IEEE, pp. 4059–4062. https://doi.org/10.1109/EMBC.2016.7591618.
Gousias, I.S., Rueckert, D., Heckemann, R.A., Dyet, L.E., Boardman, J.P., Edwards, A.D., Hammers, A., 2008. Automatic segmentation of brain MRIs of 2-year-olds into 83

regions of interest. Neuroimage 40, 672–684. https://doi.org/10.1016/J.NEUROIMAGE.2007.11.034.
Grachev, I.D., Berdichevsky, D., Rauch, S.L., Heckers, S., Kennedy, D.N., Caviness, V.S., Alpert, N.M., 1999. A method for assessing the accuracy of intersubject registration of the human brain using anatomic landmarks. Neuroimage 9, 250–268. https://doi.org/10.1006/nimg.1998.0397.
Grahn, J.A., Parkinson, J.A., Owen, A.M., Jessica, A. Grahn, John, A. Parkinson, Adrian, M. Owen, 2008. The cognitive functions of the caudate nucleus. Prog. Neurobiol. 86, 141–155. https://doi.org/10.1016/j.pneurobio.2008.09.004.
Graybiel, A.M., 1995. Building action repertoires: memory and learning functions of the basal ganglia. Curr. Opin. Neurobiol. 5, 733–741. https://doi.org/10.1016/0959-4388(95)80100-6.
Graybiel, A.M., 2000. The basal ganglia. Curr. Biol. 10, R509–R511. https://doi.org/10.1016/S0960-9822(00)00593-5.
Grazioplene, R.G., Ryman, S.G., Gray, J.R., Rustichini, A., Jung, R.E., DeYoung, C.G., 2015. Subcortical intelligence: caudate volume predicts IQ in healthy adults. Hum. Brain Mapp. 36, 1407–1416. https://doi.org/10.1002/hbm.22710.
Griffiths, K.R., Lagopoulos, J., Hermens, D.F., Lee, R.S.C., Guastella, A.J., Hickie, I.B., Balleine, B.W., 2016. Impaired causal awareness and associated cortical–basal ganglia structural changes in youth psychiatric disorders. NeuroImage Clin. 12, 285–292. https://doi.org/10.1016/j.nicl.2016.06.017.
Grimm, O., Pohlack, S., Cacciaglia, R., Winkelmann, T., Plichta, M.M., Demirakca, T., Flor, H., 2015. Amygdalar and hippocampal volume: a comparison between manual segmentation, Freesurfer and VBM. J. Neurosci. Methods 253, 254–261. https://doi.org/10.1016/j.jneumeth.2015.05.024.
Guadalupe, T., Zwiers, M.P., Teumer, A., Wittfeld, K., Vasquez, A.A., Hoogman, M., Hagoort, P., Fernandez, G., Buitelaar, J., Hegenscheid, K., Völzke, H., Franke, B., Fisher, S.E., Grabe, H.J., Francks, C., 2014. Measurement and genetics of human subcortical and hippocampal asymmetries in large datasets. Hum. Brain Mapp. 35, 3277–3289. https://doi.org/10.1002/hbm.22401.
Gui, L., Lisowski, R., Faundez, T., Hüppi, P.S., Lazeyras, F., Kocher, M., 2012. Morphology-driven automatic segmentation of MR images of the neonatal brain. Med. Image Anal. 16, 1565–1579. https://doi.org/10.1016/J.MEDIA.2012.07.006.
Guo, Z., Kashyap, S., Sonka, M., Oguz, I., 2017. Machine learning in a graph framework for subcortical segmentation. In: Styner, M.A., Angelini, E.D. (Eds.), Proceedings of SPIE-Tthe International Society for Optical Engineering, p. 101330H. https://doi.org/10.1117/12.2254874.
Habas, Piotr A., Kim, K., Corbett-Detig, J.M., Rousseau, F., Glenn, O.A., Barkovich, J.A., Studholme, C., 2010a. A spatiotemporal atlas of MR intensity, tissue probability and shape of the fetal brain with application to segmentation. Neuroimage 53, 460–470. https://doi.org/10.1016/J.NEUROIMAGE.2010.06.054.
Habas, Piotr A., Kim, K., Rousseau, F., Glenn, O.A., Barkovich, A.J., Studholme, C., 2010b. Atlas-based segmentation of developing tissues in the human brain with quantitative validation in young fetuses. Hum. Brain Mapp. 31, 1348–1358. https://doi.org/10.1002/hbm.20935.
Haber, S.N., Calzavara, R., 2009. The cortico-basal ganglia integrative network: the role of the thalamus. Brain Res. Bull. 78, 69–74. https://doi.org/10.1016/j.brainresbull.2008.09.013.
Haider, L., Simeonidou, C., Steinberger, G., Hametner, S., Grigoriadis, N., Deretzi, G., Kovacs, G.G., Kutzelnigg, A., Lassmann, H., Frischer, J.M., 2014. Multiple sclerosis deep grey matter: the relation between demyelination, neurodegeneration, inflammation and iron. J. Neurol. Neurosurg. Psychiatry 85, 1386–1395. https://doi.org/10.1136/jnnp-2014-307712.
Harrisberger, F., Buechler, R., Smieskova, R., Lenz, C., Walter, A., Egloff, L., Bendfeldt, K., Simon, A.E., Wotruba, D., Theodoridou, A., Rössler, W., Riecher-Rössler, A., Lang, U.E., Heekeren, K., Borgwardt, S., 2016. Alterations in the hippocampus and thalamus in individuals at high risk for psychosis. npj Schizophr. 2, 16033. https://doi.org/10.1038/npjschz.2016.33.
Heckemann, R.A., Hammers, A., Aljabar, P., Rueckert, D., Hajnal, J.V., 2009. The mirror method of assessing segmentation quality in atlas label propagation. In: 2009 IEEE International Symposium on Biomedical Imaging: from Nano to Macro. IEEE, pp. 1194–1197. https://doi.org/10.1109/ISBI.2009.5193272.
Heimann, T., Meinzer, H.-P., 2009. Statistical shape models for 3D medical image segmentation: a review. Med. Image Anal. 13, 543–563. https://doi.org/10.1016/j.media.2009.05.004.
Hellstrøm, T., Westlye, L.T., Sigurdardottir, S., Brunborg, C., Soberg, H.L., Holthe, Ø., Server, A., Lund, M.J., Andreassen, O.A., Andelic, N., 2017. Longitudinal changes in brain morphology from 4 weeks to 12 months after mild traumatic brain injury: associations with cognitive functions and clinical variables. Brain Inj. 31, 674–685. https://doi.org/10.1080/02699052.2017.1283537.
Helms, G., Draganski, B., Frackowiak, R., Ashburner, J., Weiskopf, N., 2009. Improved segmentation of deep brain grey matter structures using magnetization transfer (MT) parameter maps. Neuroimage 47, 194–198. https://doi.org/10.1016/J.NEUROIMAGE.2009.03.053.
Herranz, E., Giannì, C., Louapre, C., Treaba, C.A., Govindarajan, S.T., Ouellette, R., Loggia, M.L., Sloane, J.A., Madigan, N., Izquierdo-Garcia, D., Ward, N., Mangeat, G., Granberg, T., Klawiter, E.C., Catana, C., Hooker, J.M., Taylor, N., Ionete, C., Kinkel, R.P., Mainero, C., 2016. Neuroinflammatory component of gray matter pathology in multiple sclerosis. Ann. Neurol. 80, 776–790. https://doi.org/10.1002/ana.24791.
Hojjat, A., Collie, D., Colchester, A.C.F., 2002. The Putamen Intensity Gradient in CJD Diagnosis. Springer, Berlin, Heidelberg, pp. 524–531. https://doi.org/10.1007/3-540-45786-0_65.
Huo, J., Wang, G., Wu, Q.M.J., Thangarajah, A., 2015. Label Fusion for Multi-Atlas Segmentation Based on Majority Voting. Springer, Cham, pp. 100–106. https://doi.org/10.1007/978-3-319-20801-5_11.
Huo, Y., Plassard, A.J., Carass, A., Resnick, S.M., Pham, D.L., Prince, J.L., Landman, B.A., 2016. Consistent cortical reconstruction and multi-atlas brain segmentation. Neuroimage 138, 197–210. https://doi.org/10.1016/j.neuroimage.2016.05.030.
Iglesias, J.E., Sabuncu, M.R., Aganj, I., Bhatt, P., Casillas, C., Salat, D., Boxer, A., Fischl, B., Van Leemput, K., 2015. An algorithm for optimal fusion of atlases with different labeling protocols. Neuroimage 106, 451–463. https://doi.org/10.1016/j.neuroimage.2014.11.031.
Iosifescu, D.V., Shenton, M.E., Warfield, S.K., Kikinis, R., Dengler, J., Jolesz, F.A., McCarley, R.W., 1997. An automated registration algorithm for measuring MRI subcortical brain structures. Neuroimage 6, 13–25. https://doi.org/10.1006/NIMG.1997.0274.
Johnson, C.L., Schwarb, H., McGarry, M.D.J., Anderson, A.T., Huesmann, G.R., Sutton, B.P., Cohen, N.J., 2016. Viscoelasticity of subcortical gray matter structures. Hum. Brain Mapp. 37, 4221–4233. https://doi.org/10.1002/hbm.23314.
Joshi, S., Davis, B., Jomier, M., Gerig, G., 2004. Unbiased diffeomorphic atlas construction for computational anatomy. Neuroimage 23 (Suppl. 1), S151–S160. https://doi.org/10.1016/j.neuroimage.2004.07.068.
Juuhl-Langseth, M., Rimol, L.M., Rasmussen, I.A., Thormodsen, R., Holmén, A., Emblem, K.E., Due-Tønnessen, P., Rund, B.R., Agartz, I., 2012. Comprehensive segmentation of subcortical brain volumes in early onset schizophrenia reveals limited structural abnormalities. Psychiatry Res. Neuroimaging 203, 14–23. https://doi.org/10.1016/J.PSCYCHRESNS.2011.10.005.
Kang, X., Herron, T.J., Ettlinger, M., Woods, D.L., 2015. Hemispheric asymmetries in cortical and subcortical anatomy. Laterality Asymmetries Body. Brain Cogn. 20, 658–684. https://doi.org/10.1080/1357650X.2015.1032975.
Karas, G.B., Burton, E.J., Rombouts, S.A.R.B., Schijndel, R.A. van, O'Brien, J.Y., Scheltens, P., McKeith, I.G., Williams, D., Ballard, C., Barkhof, F., 2003. A comprehensive study of gray matter loss in patients with Alzheimer's disease using optimized voxel-based morphometry. Neuroimage 18, 895–907. https://doi.org/10.1016/S1053-8119(03)00041-7.
Kass, M., Witkin, A., Terzopoulos, D., Palo, S., Alto, P., 1988. Snakes: active contour models. Int. J. Comput. Vis. 1, 321–331. https://doi.org/10.1007/BF00133570.
Keuken, M.C., Bazin, P.-L., Crown, L., Hootsmans, J., Laufer, A., Müller-Axt, C., Sier, R., van der Putten, E.J., Schäfer, A., Turner, R., Forstmann, B.U., 2014. Quantifying inter-individual anatomical variability in the subcortex using 7 T structural MRI. Neuroimage 94, 40–46. https://doi.org/10.1016/J.NEUROIMAGE.2014.03.032.
Khan, A.R., Beg, M.F., 2009. Multi-structure whole brain registration and population average. In: 2009 Annual International Conference of the IEEE Engineering in Medicine and Biology Society. IEEE, pp. 5797–5800. https://doi.org/10.1109/IEMBS.2009.5335196.
Khan, A.R., Wang, L., Beg, M.F., 2008. FreeSurfer-initiated fully-automated subcortical brain segmentation in MRI using large deformation diffeomorphic metric mapping. Neuroimage 41, 735–746. https://doi.org/10.1016/j.neuroimage.2008.03.024.
Khan, A.R., Chung, M.K., Beg, M.F., 2009. Robust atlas-based brain segmentation using multi-structure confidence-weighted registration. Med. Image Comput. Comput. Assist. Interv. 12, 549–557.
Kim, E.Y., Magnotta, V.A., Liu, D., Johnson, H.J., 2014. Stable Atlas-based Mapped Prior (STAMP) machine-learning segmentation for multicenter large-scale MRI data. Magn. Reson. Imaging 32, 832–844. https://doi.org/10.1016/j.mri.2014.04.016.
Kim, G., Chu, R., Yousuf, F., Tauhid, S., Stazzone, L., Houtchens, M.K., Stankiewicz, J.M., Severson, C., Kimbrough, D., Quintana, F.J., Chitnis, T., Weiner, H.L., Healy, B.C., Bakshi, R., 2017. Sample size requirements for one-year treatment effects using deep gray matter volume from 3T MRI in progressive forms of multiple sclerosis. Int. J. Neurosci. 127, 971–980. https://doi.org/10.1080/00207454.2017.1283313.
Király, A., Szabó, N., Tóth, E., Csete, G., Faragó, P., Kocsis, K., Must, A., Vécsei, L., Kincses, Z.T., 2016. Male brain ages faster: the age and gender dependence of subcortical volumes. Brain Imag. Behav. 10, 901–910. https://doi.org/10.1007/s11682-015-9468-3.
Király, A., Szabó, N., Párdutz, Á., Tóth, E., Tajti, J., Csete, G., Faragó, P., Bodnár, P., Szok, D., Tuka, B., Pálinkás, É., Ertsey, C., Vécsei, L., Kincses, Z.T., 2018. Macro- and microstructural alterations of the subcortical structures in episodic cluster headache. Cephalalgia 38, 662–673. https://doi.org/10.1177/0333102417703762.
Kleiner-Fisman, G., Herzog, J., Fisman, D.N., Tamma, F., Lyons, K.E., Pahwa, R., Lang, A.E., Deuschl, G., 2006. Subthalamic nucleus deep brain stimulation: summary and meta-analysis of outcomes. Mov. Disord. 21, S290–S304. https://doi.org/10.1002/mds.20962.
Krämer, J., Meuth, S.G., Tenberge, J.-G., Schiffler, P., Wiendl, H., Deppe, M., 2015. Early and degressive putamen atrophy in multiple sclerosis. Int. J. Mol. Sci. 16, 23195–23209. https://doi.org/10.3390/ijms161023195.
Kremen, W.S., Prom-Wormley, E., Panizzon, M.S., Eyler, L.T., Fischl, B., Neale, M.C., Franz, C.E., Lyons, M.J., Pacheco, J., Perry, M.E., Stevens, A., Schmitt, J.E., Grant, M.D., Seidman, L.J., Thermenos, H.W., Tsuang, M.T., Eisen, S.A., Dale, A.M., Fennema-Notestine, C., 2010. Genetic and environmental influences on the size of specific brain regions in midlife: the VETSA MRI study. Neuroimage 49, 1213–1223. https://doi.org/10.1016/j.neuroimage.2009.09.043.
Kuhn, T., Schonfeld, D., Sayegh, P., Arentoft, A., Jones, J.D., Hinkin, C.H., Bookheimer, S.Y., Thames, A.D., 2017. The effects of HIV and aging on subcortical shape alterations: a 3D morphometric study. Hum. Brain Mapp. 38, 1025–1037. https://doi.org/10.1002/hbm.23436.
Kuklisova-Murgasova, M., Aljabar, P., Srinivasan, L., Counsell, S.J., Doria, V., Serag, A., Gousias, I.S., Boardman, J.P., Rutherford, M.A., Edwards, A.D., Hajnal, J.V., Rueckert, D., 2011. A dynamic 4D probabilistic atlas of the developing brain. Neuroimage 54, 2750–2763. https://doi.org/10.1016/j.neuroimage.2010.10.019.
Kushibar, K., Valverde, S., González-Villà, S., Bernal, J., Cabezas, M., Oliver, A., Lladó, X., 2019. Supervised domain adaptation for automatic sub-cortical brain structure

segmentation with minimal user interaction. Sci. Rep. 9, 6742. https://doi.org/10.1038/s41598-019-43299-z.
Lalys, F., Haegelen, C., Ferre, J.-C., El-Ganaoui, O., Jannin, P., 2010. Construction and assessment of a 3-T MRI brain template. Neuroimage 49, 345–354. https://doi.org/10.1016/j.neuroimage.2009.08.007.
Landman, B.A., Bogovic, J.A., Carass, A., Chen, M., Roy, S., Shiee, N., Yang, Z., Kishore, B., Pham, D., Bazin, P.-L., Resnick, S.M., Prince, J.L., 2013. System for integrated neuroimaging analysis and processing of structure. Neuroinformatics 11, 91–103. https://doi.org/10.1007/s12021-012-9159-9.
Larobina, M., Murino, L., Cervo, A., Alfano, B., 2015. Self-trained supervised segmentation of subcortical brain structures using multispectral magnetic resonance images. BioMed Res. Int. 2015, 1–9. https://doi.org/10.1155/2015/764383.
Lee, H., Prohovnik, I., 2008. Cross-validation of brain segmentation by SPM5 and SIENAX. Psychiatry Res. Neuroimaging 164, 172–177. https://doi.org/10.1016/j.pscychresns.2007.12.008.
Lee, Y.-W., Lee, H., Chung, I.-S., Yi, H.-A., 2017. Relationship between postural instability and subcortical volume loss in Alzheimer's disease. Medicine (Baltim.) 96, e7286. https://doi.org/10.1097/MD.0000000000007286.
Lehmann, M., Douiri, A., Kim, L.G., Modat, M., Chan, D., Ourselin, S., Barnes, J., Fox, N.C., 2010. Atrophy patterns in Alzheimer's disease and semantic dementia: a comparison of FreeSurfer and manual volumetric measurements. Neuroimage 49, 2264–2274. https://doi.org/10.1016/j.neuroimage.2009.10.056.
Lerch, J.P., Carroll, J.B., Spring, S., Bertram, L.N., Schwab, C., Hayden, M.R., Mark Henkelman, R., 2008. Automated deformation analysis in the YAC128 Huntington disease mouse model. Neuroimage 39, 32–39. https://doi.org/10.1016/j.neuroimage.2007.08.033.
Li, Y., He, H., Dong, H., Feng, X., Xie, G., Zhang, L., 2013. Discriminative analysis of early-stage Alzheimer's disease and normal aging with automatic segmentation technique in subcortical gray matter structures: a multicenter *in vivo* MRI volumetric and DTI study. Acta Radiol. 54, 1191–1200. https://doi.org/10.1177/0284185113492971.
Li, T., Zhou, F., Zhu, Z., Shu, H., Zhu, H., 2018. A label-fusion-aided convolutional neural network for isointense infant brain tissue segmentation. In: 2018 IEEE 15th International Symposium on Biomedical Imaging (ISBI 2018). IEEE, pp. 692–695. https://doi.org/10.1109/ISBI.2018.8363668.
Li, X., Chen, L., Kutten, K., Ceritoglu, C., Li, Y., Kang, N., Hsu, J.T., Qiao, Y., Wei, H., Liu, C., Miller, M.I., Mori, S., Yousem, D.M., van Zijl, P.C.M., Faria, A.V., 2019. Multi-atlas tool for automated segmentation of brain gray matter nuclei and quantification of their magnetic susceptibility. Neuroimage 191, 337–349. https://doi.org/10.1016/J.NEUROIMAGE.2019.02.016.
Liem, F., Mérillat, S., Bezzola, L., Hirsiger, S., Philipp, M., Madhyastha, T., Jäncke, L., 2015. Reliability and statistical power analysis of cortical and subcortical FreeSurfer metrics in a large sample of healthy elderly. Neuroimage 108, 95–109. https://doi.org/10.1016/j.neuroimage.2014.12.035.
Lim, I.A.L., Faria, A.V., Li, X., Hsu, J.T.C., Airan, R.D., Mori, S., van Zijl, P.C.M., 2013. Human brain atlas for automated region of interest selection in quantitative susceptibility mapping: application to determine iron content in deep gray matter structures. Neuroimage 82, 449–469. https://doi.org/10.1016/j.neuroimage.2013.05.127.
Lin, X., Qiu, T., Morain-Nicolier, F., Ruan, S., 2010. A topology preserving non-rigid registration algorithm with integration shape knowledge to segment brain subcortical structures from MRI images. Pattern Recognit. 43, 2418–2427. https://doi.org/10.1016/J.PATCOG.2010.01.012.
Linguraru, M.G., Ayache, N., Bardinet, E., Ballester, M.A.G., Galanaud, D., Haik, S., Faucheux, B., Hauw, J.-J., Cozzone, P., Dormont, D., Brandel, J.-P., 2006. Differentiation of sCJD and vCJD forms by automated analysis of basal ganglia intensity distribution in multisequence MRI of the brain-definition and evaluation of new MRI-based ratios. IEEE Trans. Med. Imaging 25, 1052–1067. https://doi.org/10.1109/TMI.2006.876133.
Linguraru, M.G., Ballester, M.Á.G., Ayache, N., 2007. Deformable atlases for the segmentation of internal brain nuclei in magnetic resonance imaging. Int. J. Comput. Commun. Control 2, 26. https://doi.org/10.15837/ijccc.2007.1.2333.
Liu, M., Kitsch, A., Miller, S., Chau, V., Poskitt, K., Rousseau, F., Shaw, D., Studholme, C., 2016. Patch-based augmentation of Expectation–Maximization for brain MRI tissue segmentation at arbitrary age after premature birth. Neuroimage 127, 387–408. https://doi.org/10.1016/j.neuroimage.2015.12.009.
Liu, Y., Wei, Y., Wang, C., 2019. Subcortical brain segmentation based on atlas registration and linearized kernel sparse representative classifier. IEEE Access 7, 31547–31557. https://doi.org/10.1109/ACCESS.2019.2902463.
Loh, W.Y., Connelly, A., Cheong, J.L.Y., Spittle, A.J., Chen, J., Adamson, C., Ahmadzai, Z.M., Fam, L.G., Rees, S., Lee, K.J., Doyle, L.W., Anderson, P.J., Thompson, D.K., 2016. A new MRI-based pediatric subcortical segmentation technique (PSST). Neuroinformatics 14, 69–81. https://doi.org/10.1007/s12021-015-9279-0.
Loh, W.Y., Anderson, P.J., Cheong, J.L.Y., Spittle, A.J., Chen, J., Lee, K.J., Molesworth, C., Inder, T.E., Connelly, A., Doyle, L.W., Thompson, D.K., 2017. Neonatal basal ganglia and thalamic volumes: very preterm birth and 7-year neurodevelopmental outcomes. Pediatr. Res. 82, 970–978. https://doi.org/10.1038/pr.2017.161.
Long, X., Liao, W., Jiang, C., Liang, D., Qiu, B., Zhang, L., 2012. Healthy aging: an automatic analysis of global and regional morphological alterations of human brain. Acad. Radiol. 19, 785–793. https://doi.org/10.1016/J.ACRA.2012.03.006.
Lorio, S., Lutti, A., Kherif, F., Ruef, A., Dukart, J., Chowdhury, R., Frackowiak, R.S., Ashburner, J., Helms, G., Weiskopf, N., Draganski, B., 2014. Disentangling in vivo the effects of iron content and atrophy on the ageing human brain. Neuroimage 103, 280–289. https://doi.org/10.1016/J.NEUROIMAGE.2014.09.044.
Lorio, S., Fresard, S., Adaszewski, S., Kherif, F., Chowdhury, R., Frackowiak, R.S., Ashburner, J., Helms, G., Weiskopf, N., Lutti, A., Draganski, B., 2016. New tissue priors for improved automated classification of subcortical brain structures on MRI. Neuroimage 130, 157–166. https://doi.org/10.1016/J.NEUROIMAGE.2016.01.062.
Lotjonen, J., Koikkalainen, J., Thurfjell, L., Rueckert, D., 2009. Atlas-based registration parameters in segmenting sub-cortical regions from brain MRI-images. In: 2009 IEEE International Symposium on Biomedical Imaging: from Nano to Macro. IEEE, pp. 21–24. https://doi.org/10.1109/ISBI.2009.5192973.
Lötjönen, J.M., Wolz, R., Koikkalainen, J.R., Thurfjell, L., Waldemar, G., Soininen, H., Rueckert, D., 2010. Fast and robust multi-atlas segmentation of brain magnetic resonance images. Neuroimage 49, 2352–2365. https://doi.org/10.1016/j.neuroimage.2009.10.026.
Lu, Y., Liang, H., Han, D., Mo, Y., Li, Z., Cheng, Y., Xu, X., Shen, Z., Tan, C., Zhao, W., Zhu, Y., Sun, X., 2016. The volumetric and shape changes of the putamen and thalamus in first episode, untreated major depressive disorder. NeuroImage Clin. 11, 658–666. https://doi.org/10.1016/j.nicl.2016.04.008.
Magnotta, V.A., Heckel, D., Andreasen, N.C., Cizadlo, T., Corson, P.W., Ehrhardt, J.C., Yuh, W.T.C., 1999. Measurement of brain structures with artificial neural networks: two- and three-dimensional applications. Radiology 211, 781–790. https://doi.org/10.1148/radiology.211.3.r99ma07781.
Magnotta, V.A., Bockholt, H.J., Johnson, H.J., Christensen, G.E., Andreasen, N.C., 2003. Subcortical, cerebellar, and magnetic resonance based consistent brain image registration. Neuroimage 19, 233–245.
Magon, S., Chakravarty, M.M., Amann, M., Weier, K., Naegelin, Y., Andelova, M., Radue, E.-W., Stippich, C., Lerch, J.P., Kappos, L., Sprenger, T., 2014. Label-fusion-segmentation and deformation-based shape analysis of deep gray matter in multiple sclerosis: the impact of thalamic subnuclei on disability. Hum. Brain Mapp. 35, 4193–4203. https://doi.org/10.1002/hbm.22470.
Magon, S., May, A., Stankewitz, A., Goadsby, P.J., Tso, A.R., Ashina, M., Amin, F.M., Seifert, C.L., Chakravarty, M.M., Müller, J., Sprenger, T., 2015. Morphological abnormalities of thalamic subnuclei in migraine: a multicenter MRI study at 3 tesla. J. Neurosci. 35, 13800–13806. https://doi.org/10.1523/JNEUROSCI.2154-15.2015.
Majid, D.S.A., Aron, A.R., Thompson, W., Sheldon, S., Hamza, S., Stoffers, D., Holland, D., Goldstein, J., Corey-Bloom, J., Dale, A.M., 2011. Basal ganglia atrophy in prodromal Huntington's disease is detectable over one year using automated segmentation. Mov. Disord. 26, 2544–2551. https://doi.org/10.1002/mds.23912.
Mak, E., Bergsland, N., Dwyer, M.G., Zivadinov, R., Kandiah, N., 2014. Subcortical atrophy is associated with cognitive impairment in mild Parkinson disease: a combined investigation of volumetric changes, cortical thickness, and vertex-based shape analysis. Am. J. Neuroradiol. 35, 2257–2264. https://doi.org/10.3174/ajnr.A4055.
Makowski, C., Béland, S., Kostopoulos, P., Bhagwat, N., Devenyi, G.A., Malla, A.K., Joober, R., Lepage, M., Chakravarty, M.M., 2018. Evaluating accuracy of striatal, pallidal, and thalamic segmentation methods: comparing automated approaches to manual delineation. Neuroimage 170, 182–198.
Makropoulos, A., Gousias, I.S., Ledig, C., Aljabar, P., Serag, A., Hajnal, J.V., Edwards, A.D., Counsell, S.J., Rueckert, D., 2014. Automatic whole brain MRI segmentation of the developing neonatal brain. IEEE Trans. Med. Imaging 33, 1818–1831. https://doi.org/10.1109/TMI.2014.2322280.
Makropoulos, A., Aljabar, P., Wright, R., Hüning, B., Merchant, N., Arichi, T., Tusor, N., Hajnal, J.V., Edwards, A.D., Counsell, S.J., Rueckert, D., 2016. Regional growth and atlasing of the developing human brain. Neuroimage 125, 456–478. https://doi.org/10.1016/j.neuroimage.2015.10.047.
Mang, S.C., Busza, A., Reiterer, S., Grodd, W., Klose, U., 2012. Thalamus segmentation based on the local diffusion direction: a group study. Magn. Reson. Med. 67, 118–126. https://doi.org/10.1002/mrm.22996.
Manjón, J.V., Coupé, P., 2016. volBrain: an online MRI brain volumetry system. Front. Neuroinform. 10, 30. https://doi.org/10.3389/fninf.2016.00030.
Marsden, C.D., Obeso, J.A., 1994. The functions of the basal ganglia and the paradox of stereotaxic surgery in Parkinson's disease. Brain 117, 877–897. https://doi.org/10.1093/brain/117.4.877.
McDonald, C.R., Hagler, D.J., Ahmadi, M.E., Tecoma, E., Iragui, V., Dale, A.M., Halgren, E., Halgren, E., 2008. Subcortical and cerebellar atrophy in mesial temporal lobe epilepsy revealed by automatic segmentation. Epilepsy Res. 79, 130–138. https://doi.org/10.1016/j.eplepsyres.2008.01.006.
Meier, D.S., Fisher, E., 2005. Atlas-based anatomic labeling in neurodegenerative disease via structure-driven atlas warping. J. Neuroimaging 15, 16–26. https://doi.org/10.1177/1051228404269493.
Meijerman, A., Amiri, H., Steenwijk, M.D., Jonker, M.A., van Schijndel, R.A., Cover, K.S., Vrenken, H., Alzheimer's Disease Neuroimaging Initiative, 2018. Reproducibility of deep gray matter atrophy rate measurement in a large multicenter dataset. AJNR. Am. J. Neuroradiol. 39, 46–53. https://doi.org/10.3174/ajnr.A5459.
Menke, R.A.L., Szewczyk-Krolikowski, K., Jbabdi, S., Jenkinson, M., Talbot, K., Mackay, C.E., Hu, M., 2014. Comprehensive morphometry of subcortical grey matter structures in early-stage Parkinson's disease. Hum. Brain Mapp. 35, 1681–1690. https://doi.org/10.1002/hbm.22282.
Mesaros, S., Rocca, M.A., Absinta, M., Ghezzi, A., Milani, N., Moiola, L., Veggiotti, P., Comi, G., Filippi, M., 2008. Evidence of thalamic gray matter loss in pediatric multiple sclerosis. Neurology 70, 1107–1112. https://doi.org/10.1212/01.wnl.0000291010.54692.85.
Messina, D., Cerasa, A., Condino, F., Arabia, G., Novellino, F., Nicoletti, G., Salsone, M., Morelli, M., Lanza, P.L., Quattrone, A., 2011. Patterns of brain atrophy in Parkinson's disease, progressive supranuclear palsy and multiple system atrophy. Park. Relat. Disord. 17, 172–176. https://doi.org/10.1016/j.parkreldis.2010.12.010.
Metzger, A., Benavides, A., Nopoulos, P., Magnotta, V., 2016. Automated tissue classification of pediatric brains from magnetic resonance images using age-specific atlases. In: Gimi, B., Krol, A. (Eds.). International Society for Optics and Photonics, p. 978820. https://doi.org/10.1117/12.2216116.

Misaki, M., Savitz, J., Zotev, V., Phillips, R., Yuan, H., Young, K.D., Drevets, W.C., Bodurka, J., 2015. Contrast enhancement by combining T1- and T2-weighted structural brain MR Images. Magn. Reson. Med. 74, 1609–1620. https://doi.org/10.1002/mrm.25560.

Moeskops, P., Viergever, M.A., Mendrik, A.M., de Vries, L.S., Benders, M.J.N.L., Isgum, I., 2016. Automatic segmentation of MR brain images with a convolutional neural network. IEEE Trans. Med. Imaging 35, 1252–1261. https://doi.org/10.1109/TMI.2016.2548501.

Moeskops, P., de Bresser, J., Kuijf, H.J., Mendrik, A.M., Biessels, G.J., Pluim, J.P.W., Išgum, I., 2018. Evaluation of a deep learning approach for the segmentation of brain tissues and white matter hyperintensities of presumed vascular origin in MRI. NeuroImage Clin. 17, 251–262. https://doi.org/10.1016/j.nicl.2017.10.007.

Möller, C., Hafkemeijer, A., Pijnenburg, Y.A.L., Rombouts, S.A.R.B., van der Grond, J., Dopper, E., van Swieten, J., Versteeg, A., Pouwels, P.J.W., Barkhof, F., Scheltens, P., Vrenken, H., van der Flier, W.M., 2015. Joint assessment of white matter integrity, cortical and subcortical atrophy to distinguish AD from behavioral variant FTD: a two-center study. NeuroImage Clin. 9, 418–429. https://doi.org/10.1016/j.nicl.2015.08.022.

Morel, A., Magnin, M., Jeanmonod, D., 1997. Multiarchitectonic and stereotactic atlas of the human thalamus. J. Comp. Neurol. 387, 588–630.

Morey, R.A., Selgrade, E.S., Wagner, H.R., Huettel, S.A., Wang, L., McCarthy, G., McCarthy, G., 2010. Scan-rescan reliability of subcortical brain volumes derived from automated segmentation. Hum. Brain Mapp. 31, 1751–1762. https://doi.org/10.1002/hbm.20973.

Narayana, P.A., Coronado, I., Robinson, M., Sujit, S.J., Datta, S., Sun, X., Lublin, F.D., Wolinsky, J.S., Gabr, R.E., 2018. Multimodal MRI segmentation of brain tissue and T2-hyperintense white matter lesions in multiple sclerosis using deep convolutional neural networks and a large multi-center image database. In: 2018 9th Cairo International Biomedical Engineering Conference (CIBEC). IEEE, pp. 13–16. https://doi.org/10.1109/CIBEC.2018.8641800.

Okubo, G., Okada, Tomohisa, Yamamoto, A., Kanagaki, M., Fushimi, Y., Okada, Tsutomu, Murata, K., Togashi, K., 2016. MP2RAGE for deep gray matter measurement of the brain: a comparative study with MPRAGE. J. Magn. Reson. Imaging 43, 55–62. https://doi.org/10.1002/jmri.24960.

Oliveira, P.P. de M., Nitrini, R., Busatto, G., Buchpiguel, C., Sato, J.R., Amaro, E., 2010. Use of SVM methods with surface-based cortical and volumetric subcortical measurements to detect Alzheimer's disease. J. Alzheimer's Dis. 19, 1263–1272. https://doi.org/10.3233/JAD-2010-1322.

Osher, S., Sethian, J.A., 1988. Fronts propagating with curvature-dependent speed: algorithms based on Hamilton-Jacobi formulations. J. Comput. Phys. 79, 12–49. https://doi.org/10.1016/0021-9991(88)90002-2.

Ostby, Y., Tamnes, C.K., Fjell, A.M., Westlye, L.T., Due-Tonnessen, P., Walhovd, K.B., 2009. Heterogeneity in subcortical brain development: a structural magnetic resonance imaging study of brain maturation from 8 to 30 years. J. Neurosci. 29, 11772–11782. https://doi.org/10.1523/JNEUROSCI.1242-09.2009.

O'Dwyer, L., Lamberton, F., Matura, S., Tanner, C., Scheibe, M., Miller, J., Rujescu, D., Prvulovic, D., Hampel, H., 2012. Reduced hippocampal volume in healthy young ApoE4 carriers: an MRI study. PLoS One 7, e48895. https://doi.org/10.1371/journal.pone.0048895.

Pal, D., Trivedi, R., Saksena, S., Yadav, A., Kumar, M., Pandey, C.M., Rathore, R.K.S., Gupta, R.K., 2011. Quantification of age- and gender-related changes in diffusion tensor imaging indices in deep grey matter of the normal human brain. J. Clin. Neurosci. 18, 193–196. https://doi.org/10.1016/J.JOCN.2010.05.033.

Patenaude, B., Smith, S.M., Kennedy, D.N., Jenkinson, M., 2011. A Bayesian model of shape and appearance for subcortical brain segmentation. Neuroimage 56, 907–922. https://doi.org/10.1016/j.neuroimage.2011.02.046.

Peelle, J.E., Cusack, R., Henson, R.N.A., 2012. Adjusting for global effects in voxel-based morphometry: gray matter decline in normal aging. Neuroimage 60, 1503–1516. https://doi.org/10.1016/j.neuroimage.2011.12.086.

Peng, Shichun, Rajapakse, J.C., 2002. Fuzzy region integration approach for subcortical structure segmentation. In: Proceedings of the 9th International Conference on Neural Information Processing, 2002. ICONIP '02. Nanyang Technol. Univ, pp. 1499–1503. https://doi.org/10.1109/ICONIP.2002.1202870.

Peng, Shichun, Liu, Jian, Yan, Guoping, 2005. Neural integration approach for subcortical structure segmentation. In: 2005 International Conference on Neural Networks and Brain. IEEE, pp. 244–248. https://doi.org/10.1109/ICNNB.2005.1614607.

Peng, S.-J., Harnod, T., Tsai, J.-Z., Ker, M.-D., Chiou, J.-C., Chiueh, H., Wu, C.-Y., Hsin, Y.-L., 2014. Evaluation of subcortical grey matter abnormalities in patients with MRI-negative cortical epilepsy determined through structural and tensor magnetic resonance imaging. BMC Neurol. 14, 104. https://doi.org/10.1186/1471-2377-14-104.

Penny, W.D., Friston, K.J., Ashburner, J.T., Kiebel, S.J., Nichols, T.E., 2011. Statistical Parametric Mapping: the Analysis of Functional Brain Images. Academic Press.

Péran, P., Cherubini, A., Luccichenti, G., Hagberg, G., Démonet, J.-F., Rascol, O., Celsis, P., Caltagirone, C., Spalletta, G., Sabatini, U., 2009. Volume and iron content in basal ganglia and thalamus. Hum. Brain Mapp. 30, 2667–2675. https://doi.org/10.1002/hbm.20698.

Perez, L., Wang, J., 2017. The Effectiveness of Data Augmentation in Image Classification Using Deep Learning.

Perlaki, G., Horvath, R., Nagy, S.A., Bogner, P., Doczi, T., Janszky, J., Orsi, G., 2017. Comparison of accuracy between FSL's FIRST and Freesurfer for caudate nucleus and putamen segmentation. Sci. Rep. 7, 2418. https://doi.org/10.1038/s41598-017-02584-5.

Petersen, R.C., Aisen, P.S., Beckett, L.A., Donohue, M.C., Gamst, A.C., Harvey, D.J., Jack, C.R., Jagust, W.J., Shaw, L.M., Toga, A.W., Trojanowski, J.Q., Weiner, M.W., Weiner, M.W., 2010. Alzheimer's disease neuroimaging initiative (ADNI): clinical characterization. Neurology 74, 201–209. https://doi.org/10.1212/WNL.0b013e3181cb3e25.

Pohl, K.M., Fisher, J., Grimson, W.E.L., Kikinis, R., Wells, W.M., 2006. A Bayesian model for joint segmentation and registration. Neuroimage 31, 228–239. https://doi.org/10.1016/j.neuroimage.2005.11.044.

Pohl, K.M., Fisher, J., Bouix, S., Shenton, M., McCarley, R.W., Grimson, W.E.L., Kikinis, R., Wells, W.M., 2007. Using the logarithm of odds to define a vector space on probabilistic atlases. Med. Image Anal. 11, 465–477. https://doi.org/10.1016/j.media.2007.06.003.

Popescu, V., Ran, N.C.G., Barkhof, F., Chard, D.T., Wheeler-Kingshott, C.A., Vrenken, H., 2014. Accurate GM atrophy quantification in MS using lesion-filling with co-registered 2D lesion masks. NeuroImage Clin. 4, 366–373. https://doi.org/10.1016/j.nicl.2014.01.004.

Postelnicu, G., Zollei, L., Fischl, B., 2009. Combined volumetric and surface registration. IEEE Trans. Med. Imaging 28, 508–522. https://doi.org/10.1109/TMI.2008.2004426.

Potvin, O., Mouiha, A., Dieumegarde, L., Duchesne, S., Alzheimer's Disease Neuroimaging Initiative, 2016. Normative data for subcortical regional volumes over the lifetime of the adult human brain. Neuroimage 137, 9–20. https://doi.org/10.1016/j.neuroimage.2016.05.016.

Powell, S., Magnotta, V., Johnson, H., Andreasen, N., 2006. Automated brain segmentation using neural networks. In: Reinhardt, J.M., Pluim, J.P.W. (Eds.). International Society for Optics and Photonics, p. 61443Q. https://doi.org/10.1117/12.651725.

Powell, S., Magnotta, V.A., Andreasen, N.C., 2007. Automated image segmentation using support vector machines. In: Pluim, J.P.W., Reinhardt, J.M. (Eds.). International Society for Optics and Photonics, p. 65122S. https://doi.org/10.1117/12.705053.

Powell, S., Magnotta, V.A., Johnson, H., Jammalamadaka, V.K., Pierson, R., Andreasen, N.C., 2008. Registration and machine learning-based automated segmentation of subcortical and cerebellar brain structures. Neuroimage 39, 238–247. https://doi.org/10.1016/j.neuroimage.2007.05.063.

Prastawa, M., Gilmore, J.H., Lin, W., Gerig, G., 2005. Automatic segmentation of MR images of the developing newborn brain. Med. Image Anal. 9, 457–466. https://doi.org/10.1016/j.media.2005.05.007.

Puonti, O., Iglesias, J.E., Van Leemput, K., 2013. Fast, sequence adaptive parcellation of brain MR using parametric models. Med. Image Comput. Comput. Assist. Interv. 16, 727–734.

Ramasamy, D.P., Benedict, R.H.B., Cox, J.L., Fritz, D., Abdelrahman, N., Hussein, S., Minagar, A., Dwyer, M.G., Zivadinov, R., 2009. Extent of cerebellum, subcortical and cortical atrophy in patients with MS. J. Neurol. Sci. 282, 47–54. https://doi.org/10.1016/j.jns.2008.12.034.

Raviv, T.R., Van Leemput, K., Wells, W.M., Golland, P., 2009. Joint segmentation of image ensembles via latent atlases. Med. Image Comput. Comput. Assist. Interv. 12, 272–280.

Raznahan, A., Shaw, P.W., Lerch, J.P., Clasen, L.S., Greenstein, D., Berman, R., Pipitone, J., Chakravarty, M.M., Giedd, J.N., 2014. Longitudinal four-dimensional mapping of subcortical anatomy in human development. Proc. Natl. Acad. Sci. U. S. A. 111, 1592–1597. https://doi.org/10.1073/pnas.1316911111.

Reid, M.W., Hannemann, N.P., York, G.E., Ritter, J.L., Kini, J.A., Lewis, J.D., Sherman, P.M., Velez, C.S., Drennon, A.M., Bolzenius, J.D., Tate, D.F., 2017. Comparing two processing pipelines to measure subcortical and cortical volumes in patients with and without mild traumatic brain injury. J. Neuroimaging 27, 365–371. https://doi.org/10.1111/jon.12431.

Rentería, M.E., Hansell, N.K., Strike, L.T., McMahon, K.L., de Zubicaray, G.I., Hickie, I.B., Thompson, P.M., Martin, N.G., Medland, S.E., Wright, M.J., 2014. Genetic architecture of subcortical brain regions: common and region-specific genetic contributions. Genes Brain Behav. 13, 821–830. https://doi.org/10.1111/gbb.12177.

Rich, A.M., Cho, Y.T., Tang, Y., Savic, A., Krystal, J.H., Wang, F., Xu, K., Anticevic, A., 2016. Amygdala volume is reduced in early course schizophrenia. Psychiatry Res. Neuroimaging 250, 50–60. https://doi.org/10.1016/j.pscychresns.2016.02.006.

Riklin-Raviv, T., Van Leemput, K., Menze, B.H., Wells III, W.M., Golland, P., 2010. Segmentation of image ensembles via latent atlases. Med. Image Anal. 14, 654–665. https://doi.org/10.1016/j.media.2010.05.004.

Ronneberger, O., Fischer, P., Brox, T., 2015. U-net: Convolutional Networks for Biomedical Image Segmentation.

Ruocco, H.H., Bonilha, L., Li, L.M., Lopes-Cendes, I., Cendes, F., 2008. Longitudinal analysis of regional grey matter loss in Huntington disease: effects of the length of the expanded CAG repeat. J. Neurol. Neurosurg. Psychiatry 79, 130–135. https://doi.org/10.1136/jnnp.2007.116244.

Rupp, J., Dzemidzic, M., Blekher, T., West, J., Hui, S., Wojcieszek, J., Saykin, A.J., Kareken, D.A., Foroud, T., 2012. Comparison of vertical and horizontal saccade measures and their relation to gray matter changes in premanifest and manifest Huntington disease. J. Neurol. 259, 267–276. https://doi.org/10.1007/s00415-011-6172-0.

Sabuncu, M.R., Yeo, B.T.T., Van Leemput, K., Fischl, B., Golland, P., 2010. A generative model for image segmentation based on label fusion. IEEE Trans. Med. Imaging 29, 1714–1729. https://doi.org/10.1109/TMI.2010.2050897.

Sacchet, M.D., Livermore, E.E., Iglesias, J.E., Glover, G.H., Gotlib, I.H., 2015. Subcortical volumes differentiate major depressive disorder, bipolar disorder, and remitted major depressive disorder. J. Psychiatr. Res. 68, 91–98. https://doi.org/10.1016/j.jpsychires.2015.06.002.

Sato, R., Shirai, T., Taniguchi, Y., Murase, T., Bito, Y., Ochi, H., 2017. Quantitative susceptibility mapping using the multiple dipole-inversion combination with k-space segmentation method. Magn. Reson. Med. Sci. 16, 340–350. https://doi.org/10.2463/mrms.mp.2016-0062.

Scherrer, Benoit, Dojat, M., Forbes, F., Garbay, C., 2009. Agentification of Markov model-based segmentation: application to magnetic resonance brain scans. Artif. Intell. Med. 46, 81–95. https://doi.org/10.1016/j.artmed.2008.08.012.
Scherrer, B., Forbes, F., Garbay, C., Dojat, M., 2009. Distributed local MRF models for tissue and structure brain segmentation. IEEE Trans. Med. Imaging 28, 1278–1295. https://doi.org/10.1109/TMI.2009.2014459.
Scott, J.A., Habas, P.A., Kim, K., Rajagopalan, V., Hamzelou, K.S., Corbett-Detig, J.M., Barkovich, A.J., Glenn, O.A., Studholme, C., 2011. Growth trajectories of the human fetal brain tissues estimated from 3D reconstructed in utero MRI. Int. J. Dev. Neurosci. 29, 529–536. https://doi.org/10.1016/j.ijdevneu.2011.04.001.
Scott, J.A., Habas, P.A., Rajagopalan, V., Kim, K., Barkovich, A.J., Glenn, O.A., Studholme, C., 2013. Volumetric and surface-based 3D MRI analyses of fetal isolated mild ventriculomegaly. Brain Struct. Funct. 218, 645–655. https://doi.org/10.1007/s00429-012-0418-1.
Sherman, S.M., Guillery, R.W., 2002. The role of the thalamus in the flow of information to the cortex. Philos. Trans. R. Soc. Lond. B Biol. Sci. 357, 1695–1708. https://doi.org/10.1098/rstb.2002.1161.
Shi, F., Yap, P.-T., Wu, G., Jia, H., Gilmore, J.H., Lin, W., Shen, D., 2011. Infant brain atlases from neonates to 1- and 2-year-olds. PLoS One 6, e18746. https://doi.org/10.1371/journal.pone.0018746.
Shi, J., Wang, Y., Ceschin, R., An, X., Nelson, M.D., Panigrahy, A., Leporé, N., 2012. Surface Fluid Registration and Multivariate Tensor-Based Morphometry in Newborns - the Effects of Prematurity on the Putamen.
Shiee, N., Bazin, P.-L., Zackowski, K.M., Farrell, S.K., Harrison, D.M., Newsome, S.D., Ratchford, J.N., Caffo, B.S., Calabresi, P.A., Pham, D.L., Reich, D.S., 2012. Revisiting brain atrophy and its relationship to disability in multiple sclerosis. PLoS One 7, e37049. https://doi.org/10.1371/journal.pone.0037049.
Shin, H.-C., Roth, H.R., Gao, M., Lu, L., Xu, Z., Nogues, I., Yao, J., Mollura, D., Summers, R.M., 2016. Deep convolutional neural networks for computer-aided detection: CNN architectures, dataset characteristics and transfer learning. IEEE Trans. Med. Imaging 35, 1285–1298. https://doi.org/10.1109/TMI.2016.2528162.
Shinohara, R.T., Oh, J., Nair, G., Calabresi, P.A., Davatzikos, C., Doshi, J., Henry, R.G., Kim, G., Linn, K.A., Papinutto, N., Pelletier, D., Pham, D.L., Reich, D.S., Rooney, W., Roy, S., Stern, W., Tummala, S., Yousuf, F., Zhu, A., Sicotte, N.L., Bakshi, R., 2017. Volumetric analysis from a harmonized multisite brain MRI study of a single subject with multiple sclerosis. Am. J. Neuroradiol. 38, 1501–1509. https://doi.org/10.3174/ajnr.A5254.
Smith, Y., Bevan, M.D., Shink, E., Bolam, J.P., 1998. Microcircuitry of the direct and indirect pathways of the basal ganglia. Neuroscience 86, 353–387. https://doi.org/10.1016/S0306-4522(98)00004-9.
Smith, S.M., Zhang, Y., Jenkinson, M., Chen, J., Matthews, P.M., Federico, A., De Stefano, N., 2002. Accurate, robust, and automated longitudinal and cross-sectional brain change analysis. Neuroimage 17, 479–489.
Solomon, A.J., Watts, R., Dewey, B.E., Reich, D.S., 2017. MRI evaluation of thalamic volume differentiates MS from common mimics. Neurol. - Neuroimmunol. Neuroinflammation 4, e387. https://doi.org/10.1212/NXI.0000000000000387.
Spilling, C.A., Jones, P.W., Dodd, J.W., Barrick, T.R., 2017. White matter lesions characterise brain involvement in moderate to severe chronic obstructive pulmonary disease, but cerebral atrophy does not. BMC Pulm. Med. 17, 92. https://doi.org/10.1186/s12890-017-0435-1.
Spoletini, I., Piras, F., Fagioli, S., Rubino, I.A., Martinotti, G., Siracusano, A., Caltagirone, C., Spalletta, G., 2011. Suicidal attempts and increased right amygdala volume in schizophrenia. Schizophr. Res. 125, 30–40. https://doi.org/10.1016/J.SCHRES.2010.08.023.
Stough, J.V., Ye, C., Ying, S.H., Prince, J.L., 2013. Thalamic parcellation from multi-modal data using random forest learning. Proceedings. IEEE Int. Symp. Biomed. Imaging 852–855. https://doi.org/10.1109/ISBI.2013.6556609.
Stüber, C., Morawski, M., Schäfer, A., Labadie, C., Wähnert, M., Leuze, C., Streicher, M., Barapatre, N., Reimann, K., Geyer, S., Spemann, D., Turner, R., 2014. Myelin and iron concentration in the human brain: a quantitative study of MRI contrast. Neuroimage 93, 95–106. https://doi.org/10.1016/J.NEUROIMAGE.2014.02.026.
Štěpán, Buksakowska, I., Szabó, N., Hořínek, D., Tóth, E., Hort, J., Warner, J., Charvát, F., Vécsei, L., Roček, M., Kincses, Z.T., 2014. Cortical and subcortical atrophy in Alzheimer disease: parallel atrophy of thalamus and hippocampus. Alzheimers Dis. Assoc. Disord. 28, 65–72. https://doi.org/10.1097/WAD.0b013e318299d3d6.
Sullivan, E.V., Pfefferbaum, A., Rohlfing, T., Baker, F.C., Padilla, M.L., Colrain, I.M., 2011. Developmental change in regional brain structure over 7 months in early adolescence: comparison of approaches for longitudinal atlas-based parcellation. Neuroimage 57, 214–224. https://doi.org/10.1016/j.neuroimage.2011.04.003.
Sunwoo, M.K., Cho, K.H., Hong, J.Y., Lee, J.E., Sohn, Y.H., Lee, P.H., 2013. Thalamic volume and related visual recognition are associated with freezing of gait in non-demented patients with Parkinson's disease. Park. Relat. Disord. 19, 1106–1109. https://doi.org/10.1016/j.parkreldis.2013.07.023.
Sussman, D., Leung, R.C., Vogan, V.M., Lee, W., Trelle, S., Lin, S., Cassel, D.B., Chakravarty, M.M., Lerch, J.P., Anagnostou, E., Taylor, M.J., 2015. The autism puzzle: diffuse but not pervasive neuroanatomical abnormalities in children with ASD. NeuroImage Clin. 8, 170–179. https://doi.org/10.1016/j.nicl.2015.04.008.
Sussman, Dafna, Leung, R.C., Chakravarty, M.M., Lerch, J.P., Taylor, M.J., 2016. The developing human brain: age-related changes in cortical, subcortical, and cerebellar anatomy. Brain Behav. 6, e00457. https://doi.org/10.1002/brb3.457.
Sussman, D., Pang, E.W., Jetly, R., Dunkley, B.T., Taylor, M.J., 2016. Neuroanatomical features in soldiers with post-traumatic stress disorder. BMC Neurosci. 17, 13. https://doi.org/10.1186/s12868-016-0247-x.
Sussman, D., da Costa, L., Chakravarty, M.M., Pang, E.W., Taylor, M.J., Dunkley, B.T., 2017. Concussion induces focal and widespread neuromorphological changes. Neurosci. Lett. 650, 52–59. https://doi.org/10.1016/j.neulet.2017.04.026.
Szczypiński, P.M., Strzelecki, M., Materka, A., Klepaczko, A., 2009. MaZda—a software package for image texture analysis. Comput. Methods Progr. Biomed. 94, 66–76. https://doi.org/10.1016/j.cmpb.2008.08.005.
Tae, W.-S., Yakunina, N., Lee, W.H., Ryu, Y.-J., Ham, H., Pyun, S.-B., Nam, E.-C., 2018. Changes in the regional shape and volume of subcortical nuclei in patients with tinnitus comorbid with mild hearing loss. Neuroradiology 60, 1203–1211. https://doi.org/10.1007/s00234-018-2093-2.
Tan, I.L., van Schijndel, R.A., Pouwels, P.J.W., Adèr, H.J., Barkhof, F., 2002. Serial isotropic three-dimensional fast FLAIR imaging: using image registration and subtraction to reveal active multiple sclerosis lesions. AJR Am. J. Roentgenol. 179, 777–782. https://doi.org/10.2214/ajr.179.3.1790777.
Tang, T., Jiao, Y., Wang, X., Lu, Z., 2013. Gender versus brain size effects on subcortical gray matter volumes in the human brain. Neurosci. Lett. 556, 79–83. https://doi.org/10.1016/j.neulet.2013.09.060.
Tang, X., Oishi, K., Faria, A.V., Hillis, A.E., Albert, M.S., Mori, S., Miller, M.I., 2013. Bayesian parameter estimation and segmentation in the multi-atlas random orbit model. PLoS One 8, e65591. https://doi.org/10.1371/journal.pone.0065591.
Tang, X., Crocetti, D., Kutten, K., Ceritoglu, C., Albert, M.S., Mori, S., Mostofsky, S.H., Miller, M.I., 2015. Segmentation of brain magnetic resonance images based on multi-atlas likelihood fusion: testing using data with a broad range of anatomical and photometric profiles. Front. Neurosci. 9, 61. https://doi.org/10.3389/fnins.2015.00061.
Tang, X., Luo, Y., Chen, Z., Huang, N., Johnson, H.J., Paulsen, J.S., Miller, M.I., 2018. A fully-automated subcortical and ventricular shape generation pipeline preserving smoothness and anatomical topology. Front. Neurosci. 12, 321. https://doi.org/10.3389/fnins.2018.00321.
Tao, G., He, R., Datta, S., Narayana, P.A., 2009. Symmetric inverse consistent nonlinear registration driven by mutual information. Comput. Methods Progr. Biomed. 95, 105–115. https://doi.org/10.1016/j.cmpb.2009.01.011.
Thirion, J.-P., 1998. Image matching as a diffusion process: an analogy with Maxwell's demons. Med. Image Anal. 2, 243–260. https://doi.org/10.1016/S1361-8415(98)80022-4.
Tinaz, S., Courtney, M.G., Stern, C.E., 2011. Focal cortical and subcortical atrophy in early Parkinson's disease. Mov. Disord. 26, 436–441. https://doi.org/10.1002/mds.23453.
Tzourio-Mazoyer, N., Landeau, B., Papathanassiou, D., Crivello, F., Etard, O., Delcroix, N., Mazoyer, B., Joliot, M., 2002. Automated anatomical labeling of activations in SPM using a macroscopic anatomical parcellation of the MNI MRI single-subject brain. Neuroimage 15, 273–289. https://doi.org/10.1006/nimg.2001.0978.
Unay, D., 2012. Local and global volume changes of subcortical brain structures from longitudinally varying neuroimaging data for dementia identification. Comput. Med. Imag. Graph. 36, 464–473. https://doi.org/10.1016/j.compmedimag.2012.03.006.
Unrath, A., Klose, U., Grodd, W., Ludolph, A.C., Kassubek, J., 2008. Directional colour encoding of the human thalamus by diffusion tensor imaging. Neurosci. Lett. 434, 322–327. https://doi.org/10.1016/j.neulet.2008.02.013.
Uzunbas, M.G., Soldea, O., Ünay, D., Çetin, M., Ünal, G., Erçil, A., Ekin, A., 2010. Coupled nonparametric shape and moment-based intershape pose priors for multiple basal ganglia structure segmentation. IEEE Trans. Med. Imaging 29, 1959–1978. https://doi.org/10.1109/TMI.2010.2053554.
van den Bogaard, S.J.A., Dumas, E.M., Ferrarini, L., Milles, J., van Buchem, M.A., van der Grond, J., Roos, R.A.C., 2011. Shape analysis of subcortical nuclei in Huntington's disease, global versus local atrophy — results from the TRACK-HD study. J. Neurol. Sci. 307, 60–68. https://doi.org/10.1016/j.jns.2011.05.015.
van den Bogaard, S.J.A., Dumas, E.M., Hart, E.P., Milles, J., Reilmann, R., Stout, J.C., Craufurd, D., Gibbard, C.R., Tabrizi, S.J., van Buchem, M.A., van der Grond, J., Roos, R.A.C., 2013. Magnetization transfer imaging in premanifest and manifest Huntington disease: a 2-year follow-up. Am. J. Neuroradiol. 34, 317–322. https://doi.org/10.3174/ajnr.A3303.
Vasconcellos, L.F., Pereira, J.S., Adachi, M., Greca, D., Cruz, M., Malak, A.L., Charchat-Fichman, H., 2018. Volumetric brain analysis as a predictor of a worse cognitive outcome in Parkinson's disease. J. Psychiatr. Res. 102, 254–260. https://doi.org/10.1016/j.jpsychires.2018.04.016.
Vaskinn, A., Hartberg, C.B., Sundet, K., Westlye, L.T., Andreassen, O.A., Melle, I., Agartz, I., 2015. Brain structure characteristics in intellectually superior schizophrenia. Psychiatry Res. Neuroimaging 232, 123–129. https://doi.org/10.1016/j.pscychresns.2015.02.005.
Veer, I.M., Oei, N.Y.L., van Buchem, M.A., Spinhoven, P., Elzinga, B.M., Rombouts, S.A.R.B., 2015. Evidence for smaller right amygdala volumes in posttraumatic stress disorder following childhood trauma. Psychiatry Res. Neuroimaging 233, 436–442. https://doi.org/10.1016/j.pscychresns.2015.07.016.
Velasco-Annis, C., Akhondi-Asl, A., Stamm, A., Warfield, S.K., 2018. Reproducibility of brain MRI segmentation algorithms: empirical comparison of local MAP PSTAPLE, FreeSurfer, and FSL-FIRST. J. Neuroimaging 28, 162–172. https://doi.org/10.1111/jon.12483.
Vidal-Jordana, A., Pareto, D., Sastre-Garriga, J., Auger, C., Ciampi, E., Montalban, X., Rovira, A., 2017. Measurement of cortical thickness and volume of subcortical structures in multiple sclerosis: agreement between 2D spin-echo and 3D MPRAGE T1-weighted images. Am. J. Neuroradiol. 38, 250–256. https://doi.org/10.3174/ajnr.A4999.
Vinitski, S., Mohamed, F., Gonzalez, C., Knobler, R., Andrews, D., Iwanaga, T., Madi, S., 1997. Fast tissue segmentation based on a 3D and 4D feature map: Comparison study, 2, 505–508.
Vinitski, S., Gonzalez, C.F., Knobler, R., Andrews, D., Iwanaga, T., Curtis, M., 1999. Fast tissue segmentation based on a 4D feature map in characterization of intracranial lesions. J. Magn. Reson. Imaging 9, 768–776. https://doi.org/10.1002/(SICI)1522-2586(199906)9:6<768::AID-JMRI3>3.0.CO;2-2.

Visser, E., Keuken, M.C., Douaud, G., Gaura, V., Bachoud-Levi, A.-C., Remy, P., Forstmann, B.U., Jenkinson, M., 2016. Automatic segmentation of the striatum and globus pallidus using MIST: multimodal Image Segmentation Tool. Neuroimage 125, 479–497. https://doi.org/10.1016/j.neuroimage.2015.10.013.

Wachinger, C., Reuter, M., Klein, T., 2018. DeepNAT: deep convolutional neural network for segmenting neuroanatomy. Neuroimage 170, 434–445. https://doi.org/10.1016/J.NEUROIMAGE.2017.02.035.

Wang, Y., Liu, T., 2015. Quantitative susceptibility mapping (QSM): decoding MRI data for a tissue magnetic biomarker. Magn. Reson. Med. 73, 82–101. https://doi.org/10.1002/mrm.25358.

Wang, H., Yushkevich, P. a, 2013a. Multi-atlas segmentation without registration: a supervoxel-based approach. Med. Image Comput. Comput. Assist. Interv. 16, 535–542.

Wang, H., Yushkevich, P.A., 2013b. Groupwise segmentation with multi-atlas joint label fusion. Med. Image Comput. Comput. Assist. Interv. 16, 711–718.

Wang, J., Vachet, C., Rumple, A., Gouttard, S., Ouziel, C., Perrot, E., Du, G., Huang, X., Gerig, G., Styner, M., 2014. Multi-atlas segmentation of subcortical brain structures via the AutoSeg software pipeline. Front. Neuroinform. 8, 7. https://doi.org/10.3389/fninf.2014.00007.

Wang, B.T., Poirier, S., Guo, T., Parrent, A.G., Peters, T.M., Khan, A.R., 2016. In: Styner, M.A., Angelini, E.D. (Eds.), Generation and Evaluation of an Ultra-high-field Atlas with Applications in DBS Planning. International Society for Optics and Photonics, p. 97840H. https://doi.org/10.1117/12.2217126.

Wang, Li, Nie, K., Zhao, X., Feng, S., Xie, S., He, X., Ma, G., Wang, Limin, Huang, Z., Huang, B., Zhang, Y., Wang, Lijuan, 2018. Characteristics of gray matter morphological change in Parkinson's disease patients with semantic abstract reasoning deficits. Neurosci. Lett. 673, 85–91. https://doi.org/10.1016/j.neulet.2017.12.047.

Warfield, S., Dengler, J., Zaers, J., Guttmann, C.R.G., Wells, W.M., Ettinger, G.J., Hiller, J., Kikinis, R., 1995. Automatic identification of gray matter structures from MRI to improve the segmentation of white matter lesions. J. Image Guid. Surg. 1, 326–38. https://doi.org/10.1002/(SICI)1522-712X(1995)1:6<326::AID-IGS4>3.0.CO;2-C.

Weisenfeld, N.I., Warfield, S.K., 2011. Learning likelihoods for labeling (L3): a general multi-classifier segmentation algorithm. Med. Image Comput. Comput. Assist. Interv. 14, 322–329.

Wenzel, F., Meyer, C., Stehle, T., Peters, J., Siemonsen, S., Thaler, C., Zagorchev, L., Alzheimer's Disease Neuroimaging Initiative, 2018. Rapid fully automatic segmentation of subcortical brain structures by shape-constrained surface adaptation. Med. Image Anal. 46, 146–161. https://doi.org/10.1016/j.media.2018.03.001.

Westman, E., Muehlboeck, J.-S., Simmons, A., 2012. Combining MRI and CSF measures for classification of Alzheimer's disease and prediction of mild cognitive impairment conversion. Neuroimage 62, 229–238. https://doi.org/10.1016/j.neuroimage.2012.04.056.

Winkelmann, T., Grimm, O., Pohlack, S.T., Nees, F., Cacciaglia, R., Dinu-Biringer, R., Steiger, F., Wicking, M., Ruttorf, M., Schad, L.R., Flor, H., 2016. Brain morphology correlates of interindividual differences in conditioned fear acquisition and extinction learning. Brain Struct. Funct. 221, 1927–1937. https://doi.org/10.1007/s00429-015-1013-z.

Wolz, R., Aljabar, P., Rueckert, D., Heckemann, R.A., Hammers, A., 2009. Segmentation of subcortical structures and the hippocampus in brain MRI using graph-cuts and subject-specific a-priori information. In: 2009 IEEE International Symposium on Biomedical Imaging: from Nano to Macro. IEEE, pp. 470–473. https://doi.org/10.1109/ISBI.2009.5193086.

Wonderlick, J.S., Ziegler, D.A., Hosseini-Varnamkhasti, P., LOCASCIO, J.J., BAKKOUR, A., van der Kouwe, A., TRIANTAFYLLOU, C., Corkin, S., DICKERSON, B.C., HOSSEINIVARNAMKHASTI, P., LOCASCIO, J.J., BAKKOUR, A., VANDERKOUWE, A., TRIANTAFYLLOU, C., Corkin, S., DICKERSON, B.C., 2009. Reliability of MRI-derived cortical and subcortical morphometric measures: effects of pulse sequence, voxel geometry, and parallel imaging. Neuroimage 44, 1324–1333.

Wu, M., Carmichael, O., Lopez-Garcia, P., Carter, C.S., Aizenstein, H.J., 2006. Quantitative comparison of AIR, SPM, and the fully deformable model for atlas-based segmentation of functional and structural MR images. Hum. Brain Mapp. 27, 747–754. https://doi.org/10.1002/hbm.20216.

Wu, M., Rosano, C., Lopez-Garcia, P., Carter, C.S., Aizenstein, H.J., 2007. Optimum template selection for atlas-based segmentation. Neuroimage 34, 1612–1618. https://doi.org/10.1016/j.neuroimage.2006.07.050.

Wu, Y., Ragin, A.B., Du, H., Sidharthan, S., Dunkle, E.E., Koktzoglou, I., Edelman, R.R., 2010. Sub-millimeter isotropic MRI for segmentation of subcortical brain regions and brain visualization. J. Magn. Reson. Imaging 31, 980–986. https://doi.org/10.1002/jmri.22120.

Wu, D., Ma, T., Ceritoglu, C., Li, Y., Chotiyanonta, J., Hou, Z., Hsu, J., Xu, X., Brown, T., Miller, M.I., Mori, S., 2016. Resource atlases for multi-atlas brain segmentations with multiple ontology levels based on T1-weighted MRI. Neuroimage 125, 120–130. https://doi.org/10.1016/j.neuroimage.2015.10.042.

XiangBo Lin, X., Su Ruan, R., Morain-Nicolier, F., TianShuang Qiu, T., 2008. Non-rigid registration based segmentation of brain subcortical structures using a priori knowledge. In: 2008 30th Annual International Conference of the IEEE Engineering in Medicine and Biology Society. IEEE, pp. 3971–3974. https://doi.org/10.1109/IEMBS.2008.4650079.

Xiao, Y., Fonov, V., Chakravarty, M.M., Beriault, S., Al Subaie, F., Sadikot, A., Pike, G.B., Bertrand, G., Collins, D.L., 2017. A dataset of multi-contrast population-averaged brain MRI atlases of a Parkinson's disease cohort. Data Br. 12, 370–379. https://doi.org/10.1016/j.dib.2017.04.013.

Yi, H.-A., Möller, C., Dieleman, N., Bouwman, F.H., Barkhof, F., Scheltens, P., van der Flier, W.M., Vrenken, H., 2016. Relation between subcortical grey matter atrophy and conversion from mild cognitive impairment to Alzheimer's disease. J. Neurol. Neurosurg. Psychiatry 87, 425–432. https://doi.org/10.1136/jnnp-2014-309105.

Yousefi, S., Kehtarnavaz, N., Gholipour, A., 2012. Improved labeling of subcortical brain structures in atlas-based segmentation of magnetic resonance images. IEEE Trans. Biomed. Eng. 59, 1808–1817. https://doi.org/10.1109/TBME.2011.2122306.

Yushkevich, P. a., Piven, J., Hazlett, H.C., Smith, R.G., Ho, S., Gee, J.C., Gerig, G., 2006. User-guided 3D active contour segmentation of anatomical structures: significantly improved efficiency and reliability. Neuroimage 31, 1116–1128. https://doi.org/10.1016/j.neuroimage.2006.01.015.

Zagorchev, L., Meyer, C., Stehle, T., Wenzel, F., Young, S., Peters, J., Weese, J., Paulsen, K., Garlinghouse, M., Ford, J., Roth, R., Flashman, L., McAllister, T., 2016. Differences in regional brain volumes two months and one year after mild traumatic brain injury. J. Neurotrauma 33, 29–34. https://doi.org/10.1089/neu.2014.3831.

Zhang, Y., Wei, G., Zhuo, J., Li, Y., Ye, W., Jiang, Ti, 2013. Regional inflation of the thalamus and globus pallidus in diving players. Med. Sci. Sport. Exerc. 45, 1077–1082. https://doi.org/10.1249/MSS.0b013e31827f4370.

Zhang, Y., Wei, H., Cronin, M.J., He, N., Yan, F., Liu, C., 2018. Longitudinal atlas for normative human brain development and aging over the lifespan using quantitative susceptibility mapping. Neuroimage 171, 176–189. https://doi.org/10.1016/J.NEUROIMAGE.2018.01.008.

Zhou, J., Rajapakse, J.C., 2005. Segmentation of subcortical brain structures using fuzzy templates. Neuroimage 28, 915–924. https://doi.org/10.1016/J.NEUROIMAGE.2005.06.037.